Development and evaluation of cancer-targeted pre-operative and intra-operative dual-imaging probes based on metal nanoparticles

（金属ナノ粒子を基盤とするがん標的術前・術中デュアルイメージングプローブの開発と評価）

2019

DING NING

Table of Contents

Abbreviations

The abbreviations used in this dissertation are as follows;

magnetic resonance imaging (MRI)

^{18}F-fluorodeoxyglucose (FDG)

positron emission tomography (PET)

indocyanine green (ICG)

photoacoustic imaging (PAI)

gold nanorods (AuNRs)

iron oxide nanoparticles (IONPs)

surface plasmon resonance (SPR)

enhanced permeability and retention (EPR)

single photon emission computed tomography (SPECT)

human epidermal growth factor receptor 2 (HER2)

1-ethyl-3-(3-dimethylaminopropyl)-carbodiimide (EDC)

N-hydroxysulfosuccinimide sodium salt (Sulfo-NHS)

2-(*N*-morpholino)ethanesulfonic acid (MES)

phosphate buffered saline (PBS)

phosphate buffered saline with Tween20 (PBST)

polyethylene glycol (PEG)

diethylenetriaminepentaacetic acid (DTPA)

sodium dodecyl sulfate (SDS)

ethylenediaminetetraacetic acid (EDTA)

transmission electron microscopy (TEM)

region of interest (ROI)

Introduction

Cancer has long been a main cause of death worldwide[1]. In Japan, cancer has been the leading cause of mortality for >30 years, and mortality rates have trended upward[2].

Among various cancer therapies, surgery remains one of the main treatments for many types of solid tumors with >50% of cancer patients undergoing surgery each year[3]. In fact, the cure rate of most solid tumor types can be increased by 4–11 folds by surgical excision[4]. To remove as much tumor tissue as possible, both highly precise pre-operative and intra-operative imaging diagnosis are necessary[5,6]. Pre-operative diagnostic techniques, such as nuclear medicine [positron emission tomography (PET) and single photon emission computed tomography (SPECT) are the representative ones] and magnetic resonance imaging (MRI), can facilitate identification of tumors. During surgeries, incomplete tumor resection remains a major challenge and occurs as much as 20% to 60% among all operations[3]. Intra-operative diagnoses, which are usually made by performing optical imaging, can identify small tumor lesions, locate metastases, help complete tumor removal, and thus guide surgeons in operating and by enabling real‑time decisions during surgery[7].

Currently, it is common to use different probes for pre-operative and intra-operative diagnosis, such as ^{18}F-fluorodeoxyglucose (FDG) for PET and indocyanine green (ICG) for fluorescence imaging[8-11], however, this might cause information discrepancies and difficulties in localization of tumors during surgery. Thus, the development of probes that could provide identical information in pre- and intra-operative diagnosis is essential for precise cancer therapy. Dual-imaging probes not only provide complementary information for diagnosis, but also bridge the gap between surgical planning and image-guided resection with a single, molecular targeting probe.

In recent years, photoacoustic imaging (PAI) has emerged as a new type of biomedical diagnostic method based on the PA effect, which is the formation of ultrasound waves following light absorption

in optical absorbers. The quantification of the sound formed by the PA effect by using transducers enables obtaining the photoacoustic signal[12]. The reconstruction of PA signals forms PA images. Ultrasound waves exhibit much lower tissue scattering, which leads to penetration depths of multiple centimeters and spatial resolution at the sub-millimeter level. Thus, PAI has the potential for a broader clinical and intra-operative application than offered by other forms of optical imaging, and development of PAI probes for tumor imaging has been strongly desired[13].

A PAI probe requires both strong absorption in the near-infrared region of the optical spectrum for high permeability through the body and generation of a strong PA response. Although there are other materials such as fluorescence dyes that can be used as PAI probes, in this study, the author chose to use metal nanoparticles [gold nanorods (AuNRs) and iron oxide nanoparticles (IONPs)] for the following reasons. First, these nanoparticles have strong and tunable optical absorptions because of the surface plasmon resonance (SPR) effect[14]. Second, the size of nanoparticles gives an advantage of much greater accumulation of the nanoparticles in tumor tissue than in normal tissues, which is known as the enhanced permeability and retention (EPR) effect[15]. Finally, many attempts have been made to modify the surfaces of metal nanoparticles, to make it possible to further optimize the accumulation and affinity toward tumor, and to easily modify the particles for applications in other pre-operative diagnostic imaging techniques for pre-operative diagnoses such as SPECT. Furthermore, IONPs themselves can be clinically utilized as an MRI probe[16].

Finally, human epidermal growth factor receptor 2 (HER2) was chosen as the target molecule for diagnosis of tumors for the following reasons: it has a close association with a poor prognosis[17]; it is highly expressed in various cancers including breast, ovarian, and gastric cancer, some of which have the highest mortality rates[18]; and HER2 is one of the most thoroughly-researched cancer-related biomarkers, which makes differential diagnosis even more necessary.

Therefore, the study aim was to develop and evaluate of HER2 positive cancer-targeted pre-

operative and intra-operative dual-imaging probes based on metal nanoparticles.

Chapter Descriptions

Chapter 1 presents the preparation and investigation of the feasibility of using radiolabeled anti-HER2 monoclonal antibody (trastuzumab)-conjugated AuNRs as PAI and SPECT probes.

Chapter 2 presents the preparation and investigation of the feasibility of using anti-HER2 scFv-IONPs as PAI and MRI probes.

Chapter 3 presents the preparation and investigation of the feasibility of using trastuzumab-conjugated liposome encapsulated with IONPs as PA and MR dual-imaging probes.

Chapter 1

Preparation and investigation of the feasibility of using radiolabeled anti-HER2 monoclonal antibody (trastuzumab)-conjugated AuNRs as PAI and SPECT probes

AuNRs were chosen as the photosensitizers. AuNRs possess an excellent photothermal conversion ability because they have strong and tunable localized surface plasmon resonance (SPR) effect[19-21]. This photothermal conversion ability ensures that AuNRs can efficiently generate PA signals, and thereby enable the use of AuNRs as an intra-operative PAI probe.

In this section, to target HER2, anti-HER2 monoclonal antibody (trastuzumab) was chosen as the ligand and conjugated to the surface of AuNRs and the compound is referred to as trastuzumab-AuNRs or Tra-AuNRs for short. To achieve pre-operative HER2 imaging, the author focused on SPECT. SPECT is a nuclear medical imaging technique widely used in clinics that enables whole-body scanning. Indium-111 (^{111}In; $t_{1/2}$ = 2.8 days; γ-radiation, 171 keV, 254 keV) is one of the commonly used radioisotopes that are applicable to SPECT imaging, and trastuzumab in Tra-AuNRs can be efficiently radiolabeled with ^{111}In by using diethylenetriaminepentaacetic acid (DTPA) as a metal chelator.

Herein, the author prepared an ^{111}In-labeled Tra-AuNRs (^{111}In-Tra-AuNRs) series that had different amounts of trastuzumab conjugated per AuNR. The binding affinities of Tra-AuNRs toward HER2 positive N87 cells were evaluated, followed by investigation of biodistribution in HER2-positive and HER2-negative tumors-bearing mice. Finally, we performed an *in vivo* SPECT imaging study using ^{111}In-Tra-AuNRs that exhibited high binding affinity to HER2 and better tumor accumulation with high background contrast.

1-1 Results and discussions

1-1-1 Characterization of ^{111}In-Tra-AuNRs series

Tra-AuNRs prepared in this study were referred to as Tra1-AuNRs, Tra2-AuNRs and Tra3-AuNRs, according to the number of trastuzumab molecules conjugated to AuNRs. The number of trastuzumab molecules conjugated to AuNRs in Tra1-, 2-, or 3-AuNRs were 0.6 ± 0.1, 2.3 ± 0.2, and 5.3 ± 0.2, respectively. The radiochemical purity of ^{111}In-Tra-AuNRs used in the following experiments was over 90%. The radiochemical yield of ^{111}In-Tra1-, 2-, and 3-AuNRs were 0.9%, 11.2%, and 0.3%, respectively.

1-1-2 Binding affinity of the Tra-AuNRs series to HER2

The dissociation constant (K_d) of the Tra-AuNRs series to HER2 was determined by measuring the absorbance of AuNRs taken up by HER2-positive N87 cells. The K_d values of Tra1-, 2-, and 3-AuNRs were 99.0 ± 54.7, 42.7 ± 15.5, and 37.7 ± 15.5 nM, respectively. The binding affinity of Tra-AuNRs series increased as the number of trastuzumab molecules conjugated to AuNRs increased, though not significantly.

1-1-3 Biodistribution of Tra-AuNRs series in tumor-bearing mice

The results of biodistribution studies of the ^{111}In-Tra-AuNRs series using N87 and SUIT2 tumor bearing mice are summarized in Tables 1-1, 1-2, and 1-3, and Figure 1-1. Only the accumulation of ^{111}In-Tra2-AuNRs at 96 h after injection showed significant differences in N87 and SUIT2 tumors, which were 9.41 ± 1.29 percentage injected dose/g tissue (%ID/g) and 5.57 ± 1.19%ID/g, respectively (Table 1-2). The mean tumor-to-blood ratio, which is an indicator of imaging contrast, was 4.18 ± 0.88 for N87 tumors which was enough to obtain high-contrast images, and was significantly higher than

that for SUIT2 tumors (2.43 ± 0.39).

In each time point, as the number of trastuzumab molecules conjugated to AuNRs increased, the accumulations in both N87 and SUIT2 tumors decreased, and faster blood clearance and higher accumulations in the liver and spleen were also observed. For instance, at 48 h after probe injection, 9.06%ID/g Tra1-AuNRs remained in blood, whereas 3.55%ID/g Tra3-AuNRs remained. In the liver, 24.79%ID/g Tra1-AuNRs remained in blood versus 39.86%ID/g Tra3-AuNRs.

High uptakes of probes by the reticuloendothelial system (RES) probably led to the lower tumor accumulations. More trastuzumab molecules conjugated to the surface of AuNRs resulted in less surface area covered with polyethylene glycol (PEG), and it has been widely reported that the introduction of antibodies to the surface of nanoparticles accompanied by less surface area of PEG leads to higher accumulation in RES[22, 23].

The Tra-AuNRs series also showed an extremely long circulation time. Within 24 h, the tumor-to-blood ratios of both N87 and SUIT2 tumors were approximately 1 (Tra1-AuNRs, N87 5.8 ± 1.0%ID/g, blood 5.4 ± 0.9%ID/g, N87/blood 1.1 ± 0.2), which made it not very suitable for clinical imaging.

Considering the results of both biodistribution and *in vitro* binding affinity of the Tra-AuNRs series to HER2, Tra2-AuNRs were chosen for the following imaging study.

Table 1-1. Biodistribution of radioactivity (%ID/g) after injection of ^{111}In-Tra1-AuNRs (n = 3).

	Time after injection of ^{111}In-Tra1-AuNRs		
	48 h	72 h	96 h
Blood	9.06 ± 4.06	5.10 ± 2.44	3.48 ± 1.08
Heart	0.83 ± 1.44	0.35 ± 0.45	1.18 ± 1.04
Lung	3.59 ± 0.50	1.46 ± 0.97	1.58 ± 0.17
Liver	24.79 ± 2.39	23.26 ± 2.51	16.97 ± 1.61
Kidney	7.13 ± 0.50	6.76 ± 1.71	4.66 ± 0.54
Stomach	0.61 ± 0.44	0.16 ± 0.18	0.19 ± 0.25
Intestine	0.98 ± 0.29	0.60 ± 0.08	0.69 ± 0.15
Pancreas	1.40 ± 0.95	0.54 ± 0.63	1.04 ± 1.15
Spleen	23.87 ± 6.03	20.14 ± 6.92	14.31 ± 3.72
Muscle	0.34 ± 0.56	0.64 ± 0.78	1.34 ± 1.49
N87	14.80 ± 4.01	14.80 ± 7.96	16.91 ± 5.78
SUIT2	11.72 ± 4.10	13.48 ± 8.01	12.26 ± 2.65

(mean ± SD)

Table 1-2. Biodistribution of radioactivity (%ID/g) after injection of ^{111}In-Tra2-AuNRs (n = 3).

	Time after injection of ^{111}In-Tra2-AuNRs		
	48 h	72 h	96 h
Blood	4.32 ± 0.55	3.80 ± 0.84	2.28 ± 0.23
Heart	0.68 ± 0.22	0.95 ± 0.40	0.27 ± 0.27
Lung	1.92 ± 0.43	1.88 ± 0.61	1.09 ± 0.05
Liver	34.20 ± 1.66	33.18 ± 1.91	26.85 ± 1.06
Kidney	8.30 ± 0.86	7.78 ± 0.82	4.76 ± 0.36
Stomach	0.49 ± 0.05	0.34 ± 0.24	0.24 ± 0.05
Intestine	0.69 ± 0.02	0.57 ± 0.11	0.38 ± 0.02
Pancreas	0.57 ± 0.13	0.50 ± 0.08	0.33 ± 0.12
Spleen	14.50 ± 5.32	14.74 ± 1.75	11.55 ± 0.86
Muscle	0.38 ± 0.20	0.61 ± 0.07	0.25 ± 0.20
N87	9.35 ± 1.47	10.80 ± 1.45	9.41 ± 1.29
SUIT2	7.44 ± 0.88	8.00 ± 0.97	5.57 ± 1.19

(mean ± SD)

Table 1-3. Biodistribution of radioactivity (%ID/g) after injection of ^{111}In-Tra3-AuNRs (n = 3).

Time after injection of ^{111}In-Tra3-AuNRs			
	48 h	72 h	96 h
Blood	3.55 ± 0.08	2.51 ± 0.97	1.77 ± 0.80
Heart	1.10 ± 0.38	0.97 ± 0.25	0.73 ± 0.39
Lung	1.83 ± 0.08	1.47 ± 0.22	0.94 ± 0.58
Liver	39.86 ± 6.71	34.71 ± 7.80	30.31 ± 10.75
Kidney	6.79 ± 0.95	5.17 ± 0.71	4.40 ± 0.94
Stomach	0.30 ± 0.15	0.50 ± 0.10	0.41 ± 0.33
Intestine	0.66 ± 0.09	0.60 ± 0.07	0.61 ± 0.19
Pancreas	0.60 ± 0.42	0.42 ± 0.12	0.57 ± 0.45
Spleen	28.06 ± 1.12	27.07 ± 7.77	21.20 ± 7.58
Muscle	0.78 ± 0.90	0.65 ± 0.74	0.81 ± 0.36
N87	5.86 ± 0.57	6.67 ± 1.67	4.39 ± 0.35
SUIT2	5.26 ± 0.47	4.38 ± 1.36	4.13 ± 1.99

(mean ± SD)

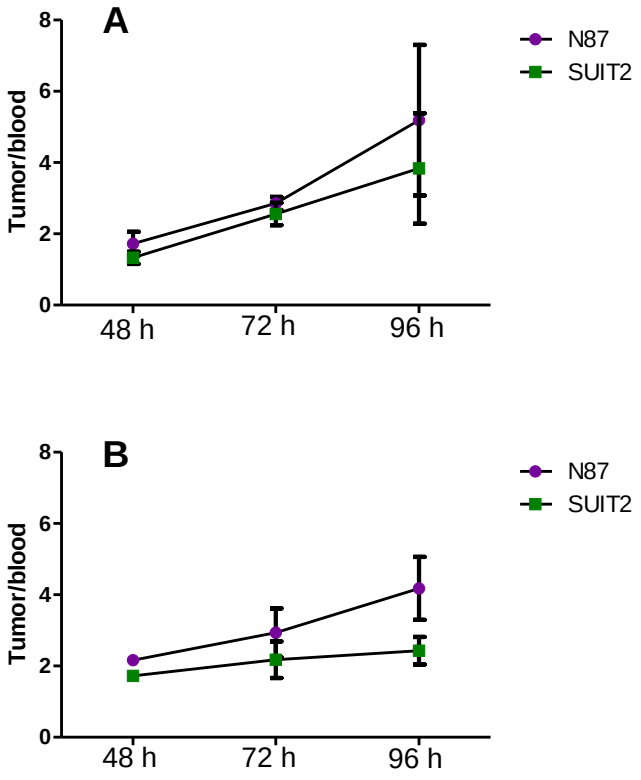

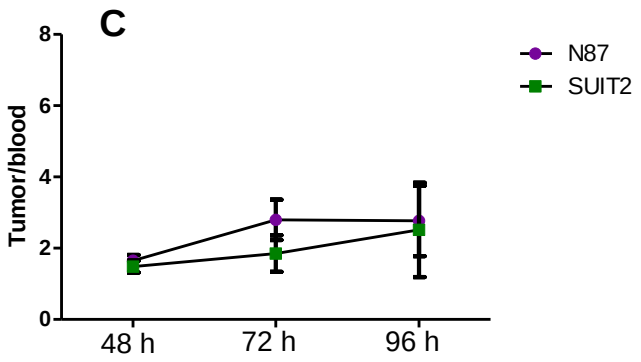

Figure 1-1. Tumor-to-blood ratios after injection of ^{111}In-Tra-AuNRs series (mean ± SD, n = 3). A: ^{111}In-Tra1-AuNRs. B: ^{111}In-Tra2-AuNRs. C: ^{111}In-Tra3-AuNRs. *p < 0.05.

1-1-4 SPECT imaging

SPECT images of tumor-bearing mice at 96 h after administration with ^{111}In-Tra2-AuNRs are shown in Figure 1-2. Compared with SUIT2 tumors at the right thighs, the N87 tumors inoculated in the left thighs were clearly visualized with high background ratios. Consistent with the data of biodistribution study data, intense signals of ^{111}In-Tra2-AuNRs were also detected in the liver.

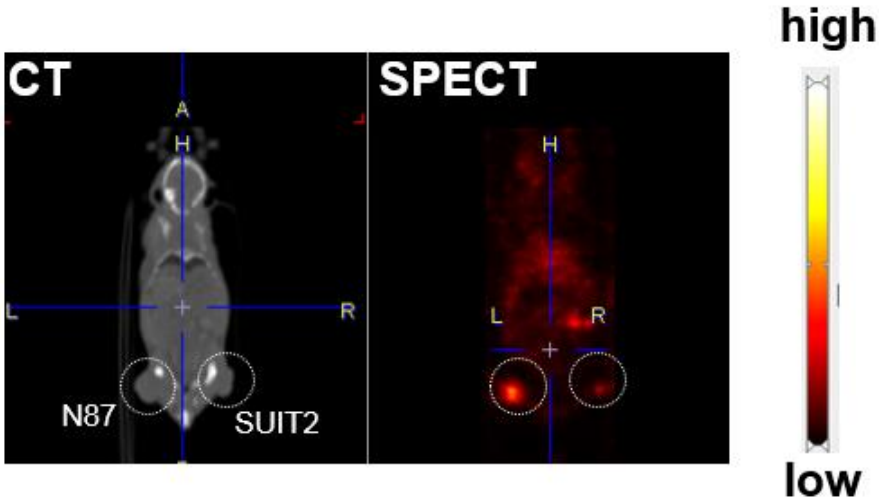

Figure 1-2. Coronal SPECT/CT images of Balb/c nude mouse inoculated with N87 (HER2 positive, left thigh) and SUIT2 (HER2 negative, right thigh) at 96 h after ^{111}In-Tra2-AuNR administration.

1-2 Summary

In this chapter, the author designed, synthesized and evaluated a series of trastuzumab-conjugated gold nanoparticles (Tra-AuNRs) labeled with ^{111}In as PA/SPECT dual-imaging probes for HER2-positive tumor imaging. These Tra-AuNRs series had different amounts of trastuzumab conjugated to AuNRs. Among the series, Tra2-AuNRs showed good binding affinity to N87 cells and the best selective accumulation to HER2 positive tumors (N87) in biodistribution studies. In the SPECT imaging study, ^{111}In-Tra2-AuNRs clearly visualized N87 tumors at 96 h after probe administration. Since it is known that AuNRs generally exhibit intense PA signals, these results suggest that Tra2-AuNRs have potential as a PA/SPECT dual-imaging probe targeting HER2-positive tumors. However, it took 96 h to obtain the high-contrast SPECT imaging of HER2 *in vivo*, so there is still room for improvement of imaging at earlier time points.

1-3 Experimental

1-3-1 Synthesis of Tra-AuNRs

Tra-AuNRs was prepared by using AuNRs (Sigma-Aldrich, St. Louis, Missouri, USA; Nanopartz, Salt Lake City, Utah, USA) and trastuzumab (Herceptin, Roche, Basel Switzerland). Trastuzumab was purified by using Amicon Ultra-4 (30 kDa) centrifugal filter units (Merck Millipore, Burlington, Massachusetts, USA) for three times at 4500×g to remove all the other excipients. 1-Ethyl-3-(3-dimethylaminopropyl)-carbodiimide (EDC, TCI Chemicals, Tokyo, Japan) and *N*-hydroxysulfosuccinimide sodium salt (Sulfo-NHS, TCI Chemicals, Tokyo, Japan) were mixed at concentrations of 0.29 and 0.21 M, respectively in 0.01 mM 2-(*N*-morpholino)ethanesulfonic acid (MES) buffer (pH 6.5) and added to 0.8 mg/mL AuNRs water solution to activate the -COOH residues

of AuNRs. After 40 min incubation at room temperature (r.t.), spared EDC and sulfo-NHS were excluded by using Amicon Ultra-4 (50 kDa) filtration two times at 3000×g. The purified trastuzumab was added to activated AuNRs and incubated under the following conditions: (i) AuNRs : trastuzumab = 1 : 67 in 0.05% phosphate buffered saline with Tween20 (PBST) (pH 7.4), 4 h at r.t.; (ii) AuNRs : trastuzumab = 1 : 329 in phosphate buffer with 0.05% Tween20 (pH 8.6), 6 h at r.t.; and (iii) AuNRs : trastuzumab = 1 : 1974 in phosphate buffer with 0.05% Tween20 (pH 8.6), 6 h at 37 °C, and the Tra-AuNRs prepared above were referred to as Tra1-AuNRs, Tra2-AuNRs and Tra3-AuNRs, respectively. After the incubation, the mixture was incubated for 1 h with NH_2-PEG (Nanocs. Inc., New York, NY, USA) and then left at 4°C overnight. Size-exclusion chromatography (AKTA Explorer, GE Healthcare, Chicago, Illinois, USA) was used to remove excess trastuzumab with Superdex 200 10/300 GL column (GE Healthcare).

1-3-2 Characterization of Tra-AuNRs

To evaluate the amount of trastuzumab conjugated to AuNRs, the following experiments were performed. Trastuzumab radiolabeled with ^{111}In was used. The purified trastuzumab was mixed with *p*-SCN-Bn-DTPA (Macrocyclics, Plano, Texas, USA) in pH 8.6 phosphate buffer at a 2:1 (*p*-SCN-Bn-DTPA: trastuzumab) reaction ratio and the reaction concentration of trastuzumab was 2.4 mg/mL. After 6 h incubation at 37°C, DTPA-trastuzumab (DTPA-Tra) was purified by using Amicon Ultra-4 (30 kDa) filtration and labeled with ^{111}In as previously described[24], followed by reaction with AuNRs as described above. Sodium dodecyl sulfate (SDS) electrophoresis followed by autoradiography was performed (Fujifilm BAS-5000, Fujifilm, Tokyo, Japan). By evaluating the radioactivity level in the regions of interest (ROIs) corresponding to AuNRs particles and free trastuzumab, the amount of trastuzumab conjugated to AuNRs was calculated.

1-3-3 Synthesis of ^{111}In-Tra-AuNRs

For biodistribution studies, ^{111}In-Tra-AuNRs series were synthesized as described in 1-3-2, followed by size-exclusion chromatography purification.

For SPECT imaging study, the purified DTPA-Tra2-AuNRs were mixed with $^{111}InCl_3$ and incubated in acetic buffer (pH 6.0) at r.t. for 60 min while shaking. After incubation, excess ethylenediaminetetraacetic acid (EDTA) (nEDTA:nDTPA = 10,000:1) was added to the mixture, and incubated at r.t. for 10 min. The mixture was purified by using a PD-10 column (GE Healthcare) and concentrated by using Amicon Ultra-4 (50 kDa) filtration at 2,150×g for twice. The final purification was performed by using size-exclusion chromatography (AKTA Explorer, GE Healthcare) with Superdex 200 10/300 GL. The radiochemical purity was determined by SDS electrophoresis as mentioned above.

1-3-4 Cell culture

NCI-N87 human gastric cancer cells (N87) (DS Pharma Biomedical, Osaka, Japan) (HER2-expressing cells) and human pancreatic cancer cells SUIT-2 (Japanese Collection of Research Bioresources Cell Bank, Osaka, Japan) (HER2-low-expressing cells) were maintained in Dulbecco's modified Eagle's medium (DMEM) (Life Technologies Co., Gaithersburg, Maryland, USA) supplemented with 10% heat-inactivated fetal bovine serum (FBS) (Life Technologies Co.), 100 U/mL penicillin, and 100 μg/mL streptomycin in a 5% CO_2/air incubator at 37°C.

1-3-5 Binding affinity of Tra-AuNRs to HER2

The binding affinities of Tra1, 2 and 3-AuNRs to HER2 were evaluated by calculating the dissociation equilibrium constant (K_d). N87 cells were seeded into 6-well plates (1.2×10^6 cells/well) and incubated in a 5% CO_2/air incubator at 37°C for 16 h. The Tra-AuNRs conjugated with different

amounts of trastuzumab were dissolved in fetal bovine serum (FBS)-free DMEM and added to cells followed by incubation for 6 h at 4°C. As a blocking group, the mixture of Tra-AuNRs and excess trastuzumab was added to cells. The AuNRs concentration in Tra-AuNRs ranged from 1 to 200 μg/mL, and the concentration of trastuzumab ranged from 5 to 150 μg/mL. After incubation, the medium was removed and the cells were washed three times by PBS at 4°C. Cells were collected and counted twice. To lyse the cells, 50 μL each of Triton X (1%) and HCl (12 N) was added. The binding of Tra-AuNRs to HER2 was confirmed by measuring the absorbance of AuNRs at 802 nm. The results of Tra1-, 2- and 3-AuNRs were compared to choose the most suitable probe.

1-3-6 Animal models

Animal studies were conducted in accordance with the institutional guidelines of Kyoto University, and the experimental procedures were approved by the Kyoto University Animal Care Committee. Five-week-old female BALB/c-*nu/nu* nude mice were purchased from Japan SLC (Shizuoka, Japan). The animals were raised in air-conditioned rooms under a 12 h light/dark cycle with free access to food and water. HER2-expressing N87 (2×10^6 cells) and HER2-low-expressing SUIT2 (1×10^6 cells) mixed with Geltrex (Life Technologies Co.) were subcutaneously inoculated into the left and right thighs of mice. Biodistribution studies and imaging studies were carried out 2 to 3 weeks after the tumor transplantation.

1-3-7 Biodistribution study

In vivo biodistribution studies were performed by using ^{111}In-labeled Tra1-, 2- and 3-AuNRs. ^{111}In-Tra-AuNRs (240 μg AuNRs) with radiochemical purity >90% in 200 μL PBS that were intravenously injected into the N87 and SUIT2 tumor-bearing mice. At 48, 72 and 96 h after injection, the organs of interest were excised and weighed; radioactivity counts were determined by using an NaI well-type

scintillation counter (1470WIZARD; PerkinElmer Co., Waltham, MA, USA) and the injected dose as a standard. Data were calculated as %ID/g. The results of Tra1, 2 and 3-AuNRs were compared to choose the most suitable probe.

1-3-8 SPECT imaging study

According to the biodistribution and affinity study results, Tra2-AuNRs were considered to be promising for *in vivo* imaging study.

^{111}In-Tra2-AuNRs (7.4 MBq, 200 μL PBS) were intravenously injected into the N87 and SUIT2 tumor-bearing mice. The mice were anesthetized with isoflurane, and SPECT/CT images were obtained by using the U-SPECT-II system (MILabs, Utrecht, the Netherlands) with 1.0-mm pinhole collimators (SPECT conditions: 30 min × 1 frame; CT conditions: accurate full angle mode in 65 kV/615 μA) at 96 h after injection. SPECT images were reconstructed by using the ordered subset expectation maximization method (8 subset, 1 iteration) with a 0.8-mm Gaussian filter.

1-3-9 Statistical Analysis

Each experiment was individually performed at least three times. The statistical significance among groups was identified by using Dunnett's test. Data are presented as the mean ± standard deviation. P values of < 0.05 were considered as indicative of statistical significance.

Chapter 2

Preparation and investigation of the feasibility of using anti-HER2 scFv-IONPs as PAI and MRI probes

Although Tra2-AuNRs demonstrated partial HER2-specific tumor accumulation *in vivo*, it was difficult to perform earlier post-injection imaging due to the slow clearance from the blood. It is reported that rod-like nanoparticles possess a longer lifetime in the blood stream than sphere-like particles[25]. AuNRs have an absorbance peak in the near-infrared (NIR) window (650–1350 nm) in which the absorbance by water and hemoglobin is at minimum[26]. However, sphere gold nanoparticles have absorbance peaks are in the range of 500–600 nm[27], which is not suitable for *in vivo* imaging. In order to overcome this problem, the author considered that IONPs, sphere-like nanoparticles approved clinically, seemed promising as a platform for PA/MR dual imaging due to the following reasons. In this research, the feasibility of using scFv-IONPs as PA/MR dual-imaging probes was investigated.

IONPs were first approved by the United States Food and Drug Administration (FDA) in 1996 (GastroMARK®) as an oral negative MR contrast agent[28] to distinguish the loops of bowel from other abdominal structures and physiology. Then onwards, other intravenous IONPs have been approved in the 2000s (such as Resovist® approved in 2001 for the European market), and have been used successfully in some instances of liver tumor enhancement due to the nonspecific uptake of the IONPs by the mononuclear phagocyte system or reticuloendothelial system (RES) after intravenous administering[29,30]. Advances in nanotechnology resulted in further systematic development of IONPs including variation in particle size and coating modification[31], and in recent years there has been renewed interests in IONPs as multifunctional vehicles[31,32]. Meanwhile, many attempts have been devoted on labeling IONPs with targeting moieties such as antibody to achieve non-invasive detection of overexpressed tumor surface antigens by MRI[31,33]. Furthermore, it is reported that IONPs, being

able to improve the sensitivity and spectroscopic specificity of a PA signal, can enhance the performance of a PA system[34]. Thus, utilizing of IONPs can lead to discrimination of tumor malignancy and determination of suitable therapeutic strategy. In fact, we previously reported that IONPs conjugated with anti-HER2 single-chain Fv (scFv) demonstrated potential as an HER2-targeted PAI probe. and a study using IONPs approved clinically as a platform for PA/MR dual imaging was conducted. In this research, the feasibility of using scFv-IONPs as PA/MR dual-imaging probes was investigated.

2-1 Results and discussion

2-1-1 Characterization of IONPs and scFv-IONPs

The scFv-IONPs were prepared by conjugation of anti-HER2 scFv to maleimide groups on the surface of nanomag®-CLD-spio. The particle size of IONPs and scFv-IONPs was 40.0 ± 8.6 and 47.5 ± 10.8 nm, respectively. Compared with unmodified IONP, the size of scFv-IONPs increased due to conjugation of the 9.7 ± 1.7 scFv molecules per IONP conjugation while the zeta potential hardly changed. The zeta potentials of IONPs and scFv-IONPs were 3.7 ± 1.5 and 3.2 ± 1.3 mV, respectively.

The transverse relaxivity (*r2*) of IONPs and scFv-IONPs was 261.6 ± 14.7, and 296.3 ± 43.3 $mM^{-1}s^{-1}$, respectively, determined by MRI machine (MRmini SA), showing no significant change due to scFv conjugation. The signal of the 0.2 mM iron concentration phantom was too low, therefore, *R2* at 0.2 mM could not be precisely measured (Figure 2-1).

The dissociation constant to HER2 (K_d) for the interaction between scFv-IONPs and HER2 was determined 11.7 ± 7.3 nM by cellular binding assay.

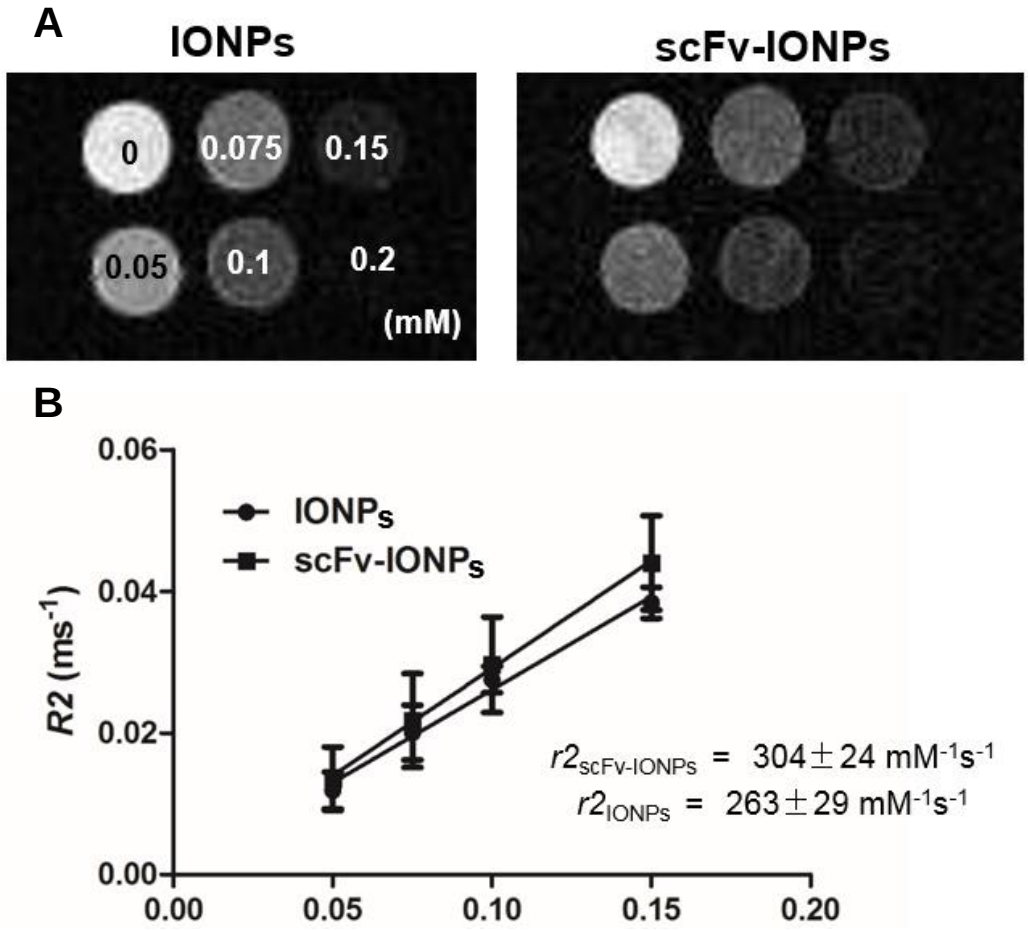

Figure 2-1. Measurement of transverse relaxivity (*r2*).

A. Representative MR images of IONPs and scFv-IONPs phantom solutions with different iron concentrations.

B. Relationship between the transverse relaxation rate (*R2*) and the iron concentration. The slope of the regression line corresponds to the transverse relaxivity (*r2*). The *r*2 values for IONPs and scFv-IONPs were 261.6 and 296.3 $mM^{-1}s^{-1}$, respectively (mean ± SD, n = 3).

2-1-2 *In vitro* MRI studies

The specific binding to HER2-overexpressing N87 cells of scFv-IONPs was further proved by *in vitro* MR studies. As described in Figure 2-2, N87 cells labeled by scFv-IONPs displayed negative contrast enhancement in *T2*-weighted MR images, in which the signal significantly decreased by 44.6 ± 7.8% than that in the control cells. This decrease in MR signal was inhibited by co-incubation of excess trastuzumab. Moreover, the MR signal of PEG-IONPs (without scFv) in N87 cells did not

change. Furthermore, the MR signal intensity was not altered by the treatment of SUIT2 cells (HER2 low expression) with scFv-IONPs. These results demonstrated the HER2-specific binding of scFv-IONPs *in vitro*.

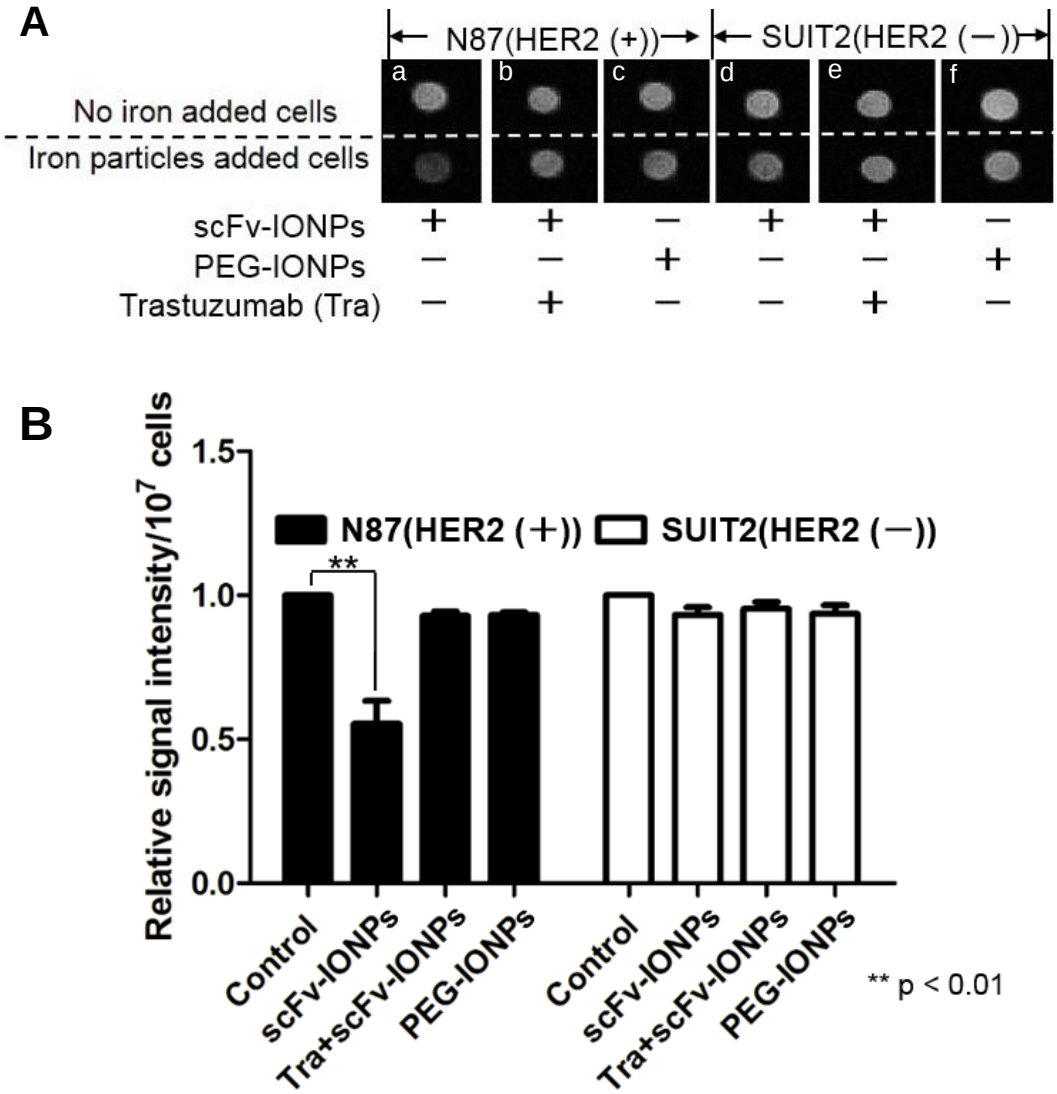

Figure 2-2. *In vitro* cellular binding assay of the IONPs conjugated with or without anti-HER2 scFv.
A. Representative MR images of the cells collected in tubes. a. scFv-IONP in N87; b. scFv-IONP (trastuzumab pre-treated) in N87; c. PEG-IONP in N87; d. scFv-IONP in SUIT2; e. scFv-IONP (trastuzumab pre-treated) in SUIT2; f. PEG-IONP in SUIT2.
B. The relative MR signal intensity per 10^7 cells calculated from *in vitro* MR images (mean ± SD, n = 3). ** $p < 0.01$ vs Control.

2-1-3 *In vivo* MRI studies

MR images were acquired with scFv-IONPs or PEG-IONPs in the N87 and SUIT2 tumor-bearing mice. At 24 h after injection of scFv-IONPs, MR signals in the N87 tumors significantly decreased than that in the SUIT2 (Figure 2-3A). Meanwhile, less decrease in the signal of PEG-IONPs was observed in both N87 and SUIT2 tumors. The percentage of signal decrease was 19.3 ± 5.3%, 8.4 ± 2.6%, 6.2 ± 2.5%, and 5.1 ± 1.3%, for scFv-IONPs in N87 tumor, PEG-IONPs in N87 tumor, scFv-IONPs in SUIT2 tumor, and PEG-IONPs in SUIT2 tumor, respectively (Figure 2-3B). As for the *in vivo* blocking study, the accumulation of scFv-IONPs in N87 tumors was inhibited by co-injection of excess trastuzumab and the signal decrease was 10.2 ± 3.7% and 4.2 ± 2.7% for N87 and SUIT2 tumor, respectively. The scFv-IONPs statistically demonstrated HER2-specific tumor uptake and the decrease in MR signals *in vivo* as well as *in vitro*.

Meanwhile, although the MR signal changes of scFv-IONPs and PEG-IONPs injected N87 tumors were significantly different ($p < 0.01$), MR signals could be seen decreased in PEG-IONPs-administered N87 tumors as well (Figure 2-3B). This is partially due to non-specific tumor uptake *via* EPR effect and by tumor-associated macrophages presenting in most tumors[35,36]. It suggested that further modification to enhance tumor accumulation as well as lower particle opsonization[9] would be required in order to be employed in MR diagnosis.

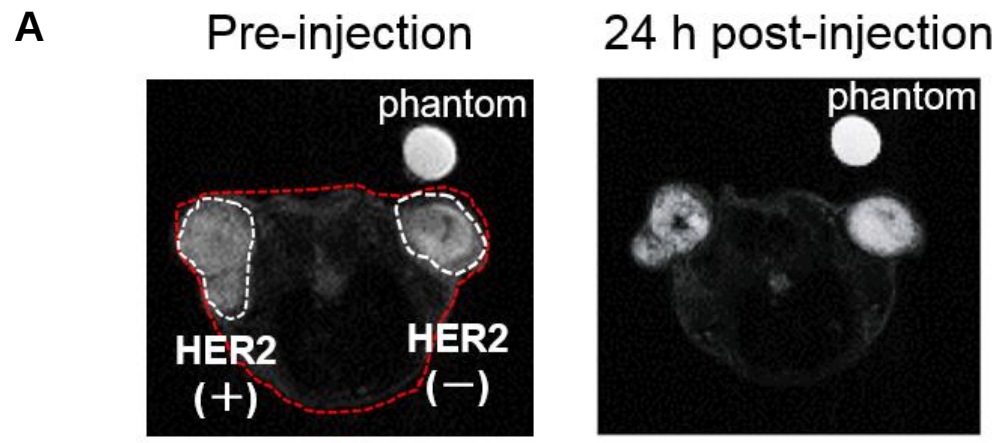

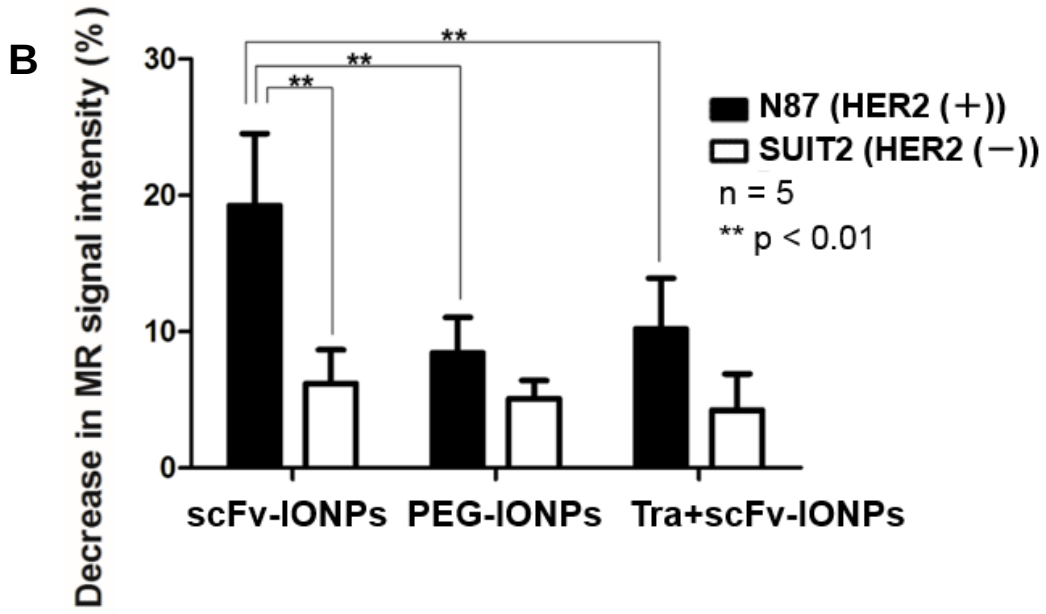

Figure 2-3. *In vivo* MR tumor imaging with scFv-IONPs or PEG-IONPs in N87 and SUIT2 tumor-bearing mice.

A. *In vivo* MR images (transverse plane) of scFv-IONP in N87 (HER2 (+)) and SUIT2 (HER2 (-)) tumor bearing mice. The red line showed the outline of mouse's body in transverse plane, and the white circles indicated transplanted tumors.

B. Decrease in MR signal intensity calculated from *in vivo* MR images using the following equation: Decrease in MRI signal (%) = $[1-({}_{post}ROI_{tumor}/{}_{post}ROI_{phantom})/({}_{pre}ROI_{tumor}/{}_{pre}ROI_{phantom})]\times100$ (mean ± SD, n = 5). **p < 0.01.

2-1-4 IONPs staining

In order to evaluate the uptake of IONPs in the tumor, iron staining of tumor sections was carried out. The slices of N87 and SUIT2 tumors excised from the mice injected with scFv-IONPs or PEG-IONPs were stained using Berlin blue staining set (Figure 2-4). The blue spots derived from IONPs were notable in N87 tumor that was injected with scFv-IONPs and the accumulation was obviously higher than that in the SUIT2 tumor (Figure 2-4A and B). Meanwhile, low amount of IONPs was observed in both N87 and SUIT2 tumor injected with PEG-IONPs (Figure 2-4C and D), which was consistent with the *in vivo* MR studies and our previous report.

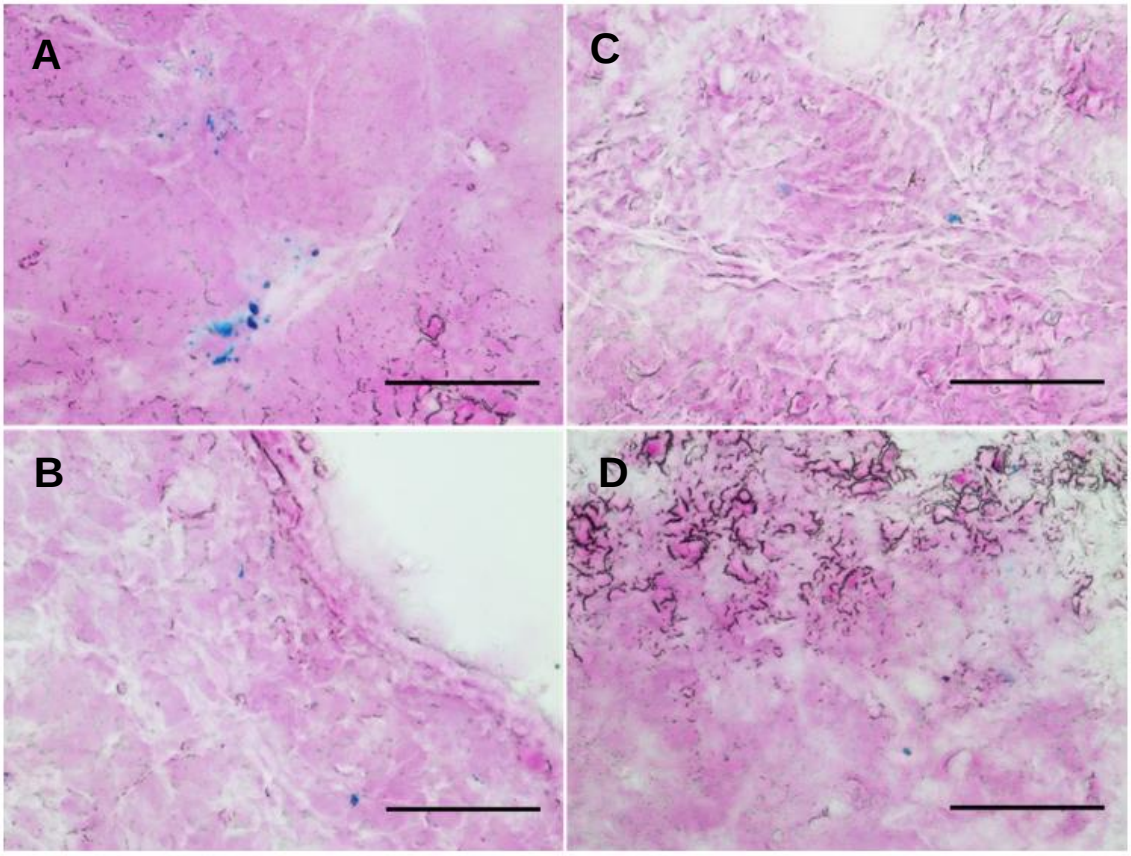

Figure 2-4. *Ex vivo* IONP distribution in the tumor.

The tumors were excised from N87 and SUIT2 tumor-bearing mice injected with scFv-IONPs or PEG-IONPs. Iron staining using Berlin blue and nucleus staining using Nuclear fast red was performed. Scale bar = 100 μm.

A. N87 tumor excised from mice injected with scFv-IONPs.

B. SUIT2 tumor excised from mice injected with scFv-IONPs.

C. N87 tumor excised from mice injected with PEG-IONPs.

D. SUIT2 tumor excised from mice injected with PEG-IONPs.

2-2 Summary

In this chapter, the author designed, synthesized and evaluated anti-HER2 single chain Fv-conjugated iron oxide nanoparticles (scFv-IONPs) as MRI probes. In phantom study, scFv-IONPs showed high transverse relaxivity. In binding affinity study, high affinity to HER2 positive cells was confirmed. The scFv-IONPs also significantly decreased both *in vitro* and *in vivo* MR signals in the

HER2 positive N87 cells and N87 tumors. Together with the conclusion from our previous studies on the scFv-IONPs' potential as a PAI agent, these results suggest that scFv-IONPs would serve as a robust cancer-targeted PA/MR dual imaging probe.

2-3 Experimental

2-3-1 Synthesis of anti-HER2 scFv-conjugated iron oxide nanoparticles (scFv-IONPs)

ScFv-IONPs were prepared according to our previous report[37] by using nanomag®-CLD-spio (diameter 20 nm, Corefront Co. (Tokyo, Japan)) instead of nanomag®-D-spio (diameter 20 nm, Corefront Co., Tokyo, Japan)). In order to conjugate anti-HER2 scFv to iron oxide nanoparticles by forming thioether bond with maleimide groups on the particle surface, anti-HER2 scFv was reduced using tris(2-carboxyethyl)phosphine (Thermo Fisher Scientific Inc., Waltham, MA, USA) for 2 h followed by mixing with iron oxide nanoparticles nanomag®-CLD-spio and incubation at r.t. for 4 h. After anti-HER2 scFv was conjugated to nanomag®-CLD-spio, thiol PEG (MW = 1000, Nanocs. Inc., New York, NY, USA) was added to the mixture to quench the maleimide groups of the particles followed by 1 h of incubation at r.t. and overnight incubation at 4°C. The mixture was electrophoresed to determine the amount of unreacted scFv. The number of anti-HER2 scFv bound to IONPs was quantified by subtracting unconjugated anti-HER2 scFv from the total amount of scFv added. To remove the unreacted scFv, the mixture was purified by dialyzing against PBS with Float-A-Lyzer® G2 (Spectra/Por®, MWCO 300 kDa, SpectrumLabs Com., Rancho Dominguez, CA, USA).

On the other hand, as a control probe, IONPs conjugated with PEG (PEG-IONPs) were prepared by reacting nanomag®-CLD-spio with thiol PEG followed by incubation at r.t. for 1 h and incubation at 4°C overnight and was purified in the same way as scFv-IONPs.

2-3-2 Physicochemical properties of scFv-IONPs

The particle size and zeta potential were measured by Zetasizer Nano ZS (Malvern Instruments, Ltd., Worcestershire, UK) both at 25°C in PBS. The concentration of iron in the particles was measured as previously described[35].

2-3-3 Calculation of *r2*

To measure the transverse relaxivity (*r2*) of scFv-IONPs, phantom studies were performed using a MR system designed for small animals (MRmini SA (1.5 T), DS Pharma Biomedical, Osaka, Japan). Nanomag®-CLD-spio and scFv-IONPs were diluted in PBS with iron concentrations ranging from 0 to 0.2 mM. The solutions were put into the φ38.5 mm RF coil and imaged using a 2-dimentional multi-slice *T2*-weighted sequence (2D-MS, *T2*W). The parameters are as follows. Average = 4; pulse repetition time (TR) = 2000 ms; echo time (TE) = 70, 100, 150, and 200 ms; slice thickness = 1 mm; slice number = 15; field of view = 30×60 mm^2; matrix size = 256×128; flip angle = 90°. Using ImageJ software, the region of interest (ROI) of each solution was drawn and the signal intensity was measured. *R2* was obtained by fitting the logarithm of MR signal intensity vs TE, and *r2* was obtained from the slope of the regression line between *R2* and concentrations of IONPs or scFv-IONPs.

2-3-4 Cell culture

Cell culture of N87 and SUIT2 cells were performed according to the method in Chapter 1.

2-3-5 Binding affinity of scFv-IONPs to HER2

The binding affinity of scFv-IONPs to HER2 was evaluated by calculating the K_d values. HER2-expressing N87 cells were seeded in 24-well plate (4×10^5 cells/well) and incubated in a 5% CO_2/air incubator at 37°C for 16 h. The scFv-IONPs were dissolved in FBS-free DMEM and added to cells

followed by incubation for 1 h at 4°C. As a blocking group, the mixture of scFv-IONPs and excess trastuzumab was added to cells. The iron concentration of scFv-IONPs ranged from 1 to 200 μg/mL, while the concentration of trastuzumab ranged from 4 to 800 μg/mL (n_{scFv}: $n_{trastuzumab}$ = 1:100). After incubation, DMEM was removed and cells were washed twice by PBS at 4°C. Triton X (1%) and HCl (12 M) was added as 100 μL/well to lyse the cells and to denature the iron particles. The binding of scFv-IONPs to HER2 was confirmed by measuring the amount of iron, which was determined based on the absorbance at 535 nm as mentioned previously.

2-3-6 *In vitro* MRI studies

N87 or SUIT-2 cells were cultured in 75 cm^2 flask (1×10^7 cells) for 16 h, followed by removal of the medium and washing twice with PBS. The scFv-IONPs or PEG-IONPs in FBS-free DMEM medium was added to the flask (m_{iron} = 0.5 μg). For blocking studies, N87 and SUIT2 cells were pre-incubated with trastuzumab in FBS-free DMEM medium ($m_{trastuzumab}$ = 20 μg, n_{scFv}:$n_{trastuzumab}$ = 1:1000) for 1 h before the addition of scFv-IONPs to the flasks. After 4 h incubation at 37°C, 1×10^7 cells were collected in tubes, and additionally washed twice with PBS. N87 or SUIT2 cells without added IONPs were collected as control. The centrifuged cells were put into φ38.5 mm RF coil of MRmini SA, and images were taken under the following condition: 2D-MS, *T2*W, Average = 4; TR = 2000 ms; TE = 70 ms; slice thickness = 1 mm; slice number = 33. ROI of cells in each tube was selected and the signal intensity was measured using ImageJ software.

2-3-7 *In vivo* MRI studies

N87 and SUIT2 tumors-bearing mice were prepared according to the method in Chapter 1. The scFv-IONPs or PEG-IONPs (60 mg iron/kg (33.2 nmol IONP/kg), 200 μL) were injected into the tumor-bearing mice *via* the tail vein. For *in vivo* blocking studies, the mixture of scFv-IONPs and

trastuzumab (24 mg/kg, n_{scFv}:$n_{trastuzumab}$ = 1:10) was intravenously injected into mice. MR images were taken with φ30 mm RF coil of MRmini SA before injection and 24 h after injection under the following condition: 2D-MS, *T2*W, Average = 4; TR = 4000 ms; TE = 70 ms; slice thickness = 2 mm; slice number = 17. The time point was decided based on our previous result that the highest accumulation of scFv-IONPs in N87 tumor along with the high tumor-to-blood ratio was observed 24 h after intravenous injection[34]. Water was used as a signal reference. ROI of each slice of tumors was drawn and the signal intensity was measured using ImageJ software. The ratio of tumor-to-phantom in each slice was calculated, and then post/pre-injection ratios were analyzed. The percentage of decrease in MR signal ($[1-({}_{post}ROI_{tumor}/{}_{post}ROI_{phantom})/({}_{pre}ROI_{tumor}/{}_{pre}ROI_{phantom})]\times100\%$) was calculated and shown in Figure 2-3.

2-3-8 IONPs staining

After *in vivo* MR studies, the mice injected with scFv-IONPs or PEG-IONPs were sacrificed, and the N87 and SUIT2 tumors were excised. The excised tumors were frozen, and cut into 10-μm-thick sections. Iron staining was performed using Berlin blue staining set (Wako Pure Chemical Industries, Ltd., Osaka, Japan). The tumor slices were then stained with Nuclear fast red (Sigma-Aldrich Co., St. Louis, MO, USA) and observed with microscope (BIOREVO BZ-9000, KEYENCE Co., Osaka, Japan).

2-3-9 Statistical analysis

Each experiment was performed at least thrice. For the *in vivo* experiment n = 5 mice were used. Statistical significance among groups was identified using the Dunnett method and Tukey-Kramer method for *in vitro* and *in vivo* experiments respectively. Data are presented as the mean ± standard deviation. *P* values of less than 0.05 were considered statistically significant.

Chapter 3

Preparation and investigation of the feasibility of using trastuzumab-conjugated liposomes encapsulated with IONPs as PA and MR dual-imaging probes

In Chapter 2, we described IONPs conjugated with anti-HER2 antibody derivatives (scFv-IONPs), which have been reported as potential probes for both PAI and MRI[37,38]. The probe showed HER2-specific tumor uptake, whereas > 10 times the amount of IONPs was needed to achieve PA tumor imaging than needed by MRI, which indicated the need to improve the imaging sensitivity of the probe, especially when used as a PAI probe.

Multiple studies have reported the marked enhancement of PA signals when the PA probes form aggregates[39,40]. A possible enhancement process is that when a nanomaterial with a high thermal conductivity absorbs light energy delivered by nanosecond laser pulses, heat occurs inside the nanomaterial, and it is quickly transferred to the surrounding medium. The thermal flux results in a thermal field around a single nanomaterial. In this case, the PA signal produced from a nanomaterial stems from the thermoelastic expansion that occurs when the surrounding medium is locally heated. The close proximity of an aggregate nanomaterial may result in overlapping thermal fields. This overlap would lead to amplification of the PA signal because overlapping thermal fields cause an increase in the rate of thermal flux and the enhancement of the PA signal strength[41-43].

These facts indicate that the density of PA probes might be a key factor in determining the sensitivity of PA signals. Therefore, we designed and synthesized PA probes having IONPs inside liposomes at a high concentration and then conjugated anti-HER2 monoclonal antibody (trastuzumab) to the surface of liposomes (Tra-Lipo-IONPs) for targeting HER2-positive tumors. In this chapter, the sensitivity of IONPs-containing liposome and intact IONPs for PAI/MRI was evaluated, and the feasibility of a

HER2-specific PA/MR dual imaging probe was investigated *in vitro* and *in vivo*.

3-1 Results and discussion

3-1-1 Physicochemical properties and transmission electron microscope (TEM) characterization of Tra-Lipo-IONPs

The physicochemical properties of Tra-Lipo-IONPs are summarized in Table 3-1. As the reactant concentration of trastuzumab increased, the amount of trastuzumab covalently bound to liposomes increased accordingly. These are referred to as Tra0-Lipo-IONP (no trastuzumab modification), Tra60-Lipo-IONP (final trastuzumab concentration 60.4 μg/mL) and Tra300-Lipo-IONP (final trastuzumab concentration 293.2 μg/mL) respectively. The size of Tra-Lipo-IONPs was approximately 80 nm, and no significant size increase was observed due to trastuzumab conjugation. The zeta potentials of all liposomes were around -80 mV, suggesting negatively charged nanoparticles. There were no significant differences in the ratio of encapsulated IONPs (mg) and lipids (mg) in different Tra-Lipo-IONPs (approximately 0.7 for all Tra-Lipo-IONPs).

It was clearly shown in TEM images that a considerable amount of IONPs were encapsulated inside liposomes, whose size was less than 100 nm, corresponding to the data measured by dynamic light scattering (Figure 3-1, Table 3-1).

Table 3-1. Physicochemical properties of Tra0, 60, and 300-Lipo-IONPs.

Probe	Lipid Concentration (mg/mL)	Iron Concentration (mg/mL)	Iron/lipid (mg/mg)	Trastuzumab Concentration (μg)/mL	Size (nm)	ζ potential (mV)
Tra0-Lipo-IONPs	48.9	33.9	0.69	0	79.2	-82
Tra60-Lipo-IONPs	54.7	36.2	0.66	60.4	83.4	-83
Tra300-Lipo-IONPs	68.2	49	0.72	293.2	76.5	-84

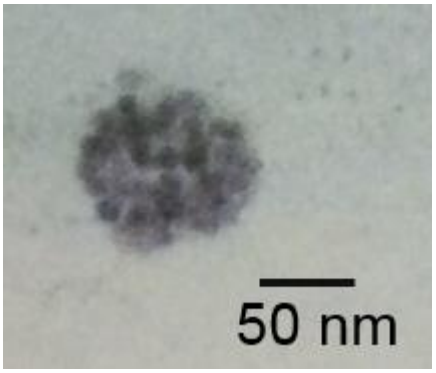

Figure 3-1. A representative TEM image of liposome encapsulated with IONPs.

3-1-2 Photoacoustic signal measurement

The basic PA characteristics of all Tra-Lipo-IONPs and IONPs were measured. With IONPs encapsulated inside liposomes, the PA signal increased 2.6-fold, compared to dispersed IONPs at the same iron concentration (Figure 3-2A). In addition, conjugation of trastuzumab to liposomes did not cause significant changes to PA signals.

3-1-3 Calculation of *r2*

The *r2* of IONPs and Tra0-Lipo-IONPs was 386 and 102 $mM^{-1}s^{-1}$, respectively (Figure 3-2B). Similar to the results of PA phantom signals, Tra0-Lipo-IONPs with capsulated IONPs exhibited higher *r2*; in other words, stronger negative contrast enhancement, compared to dispersed IONPs at the same iron concentration.

Lipo-IONPs were designed and prepared with a large amount of IONPs compacted inside an aqueous-phased environment. Having IONPs compacted inside liposomes is similar to having a larger-sized particle, which brings higher magnetic moments[44]. Furthermore, the compacted IONPs and interior aqueous phase together guarantee that the spin-spin relaxation process of protons in the water molecules surrounding the nanocrystals is facilitated by the magnitude of magnetic spins in

nanocrystals; it is reasonable to observe darker MR images[45].

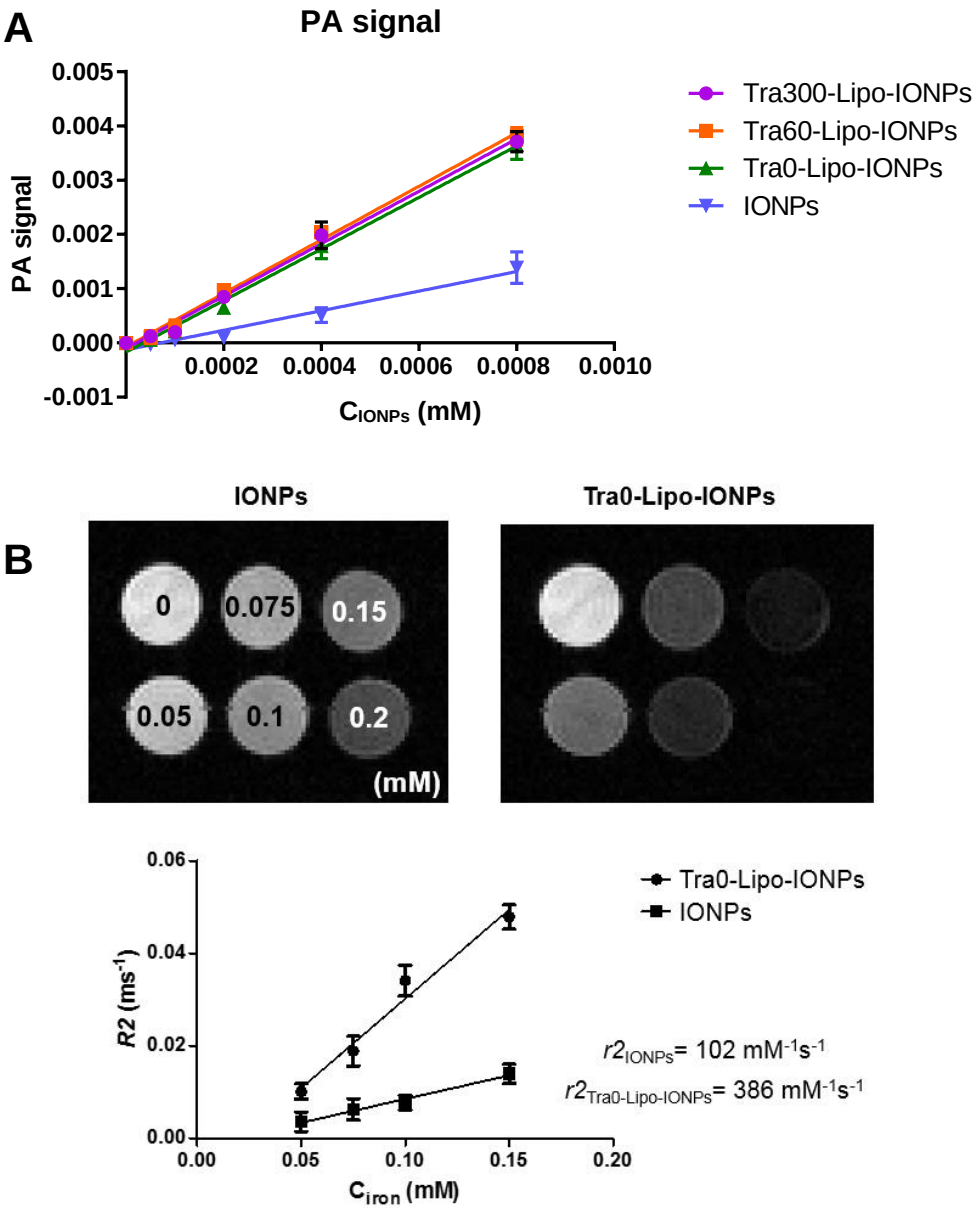

Figure 3-2. A. PA signals of IONPs and Tra-Lipo-IONPs (mean ± SD, n = 3). PA signals are plotted against IONPs concentration. B. Measurement of *r2* of IONPs and Tra-Lipo-IONPs (mean ± SD, n = 3). Representative MR images of IONP phantom solutions with different iron concentrations (0-0.2 mM). Relationship between transverse relaxation rate (*R2*) and iron concentration. The slope of the regression line corresponds to the transverse relaxivity (*r2*). The *r2* values for IONPs and Tra-Lipo-IONPs were 386 and 102 $mM^{-1}s^{-1}$, respectively.

3-1-4 *In vitro* fluorescence microscopy study and iron staining

In HER2-overexpressing N87 cells, the fluorescence signals increased with time when treated with Tra-Lipo-IONPs (Figure 3-3). As the amount of trastuzumab conjugated to the liposome surface increased, the fluorescence signals were enhanced (the most intense signals were observed in N87 cells treated with Tra300-Lipo-IONPs for 6 h). Low fluorescence signals were observed in N87 cells treated with Tra0-Lipo-IONPs, in N87 cells treated with Tra60, or 300-Lipo-IONPs, along with an excess amount of trastuzumab, and in SUIT2 cells treated with Tra60 or 300-Lipo-IONPs, demonstrating HER2-specific binding of Tra-Lipo-IONPs *in vitro*.

Furthermore, positive fluorescence regions were coincident with iron-positive regions, suggesting the co-localization of lipids forming the liposomes and IONPs encapsulated in the liposomes.

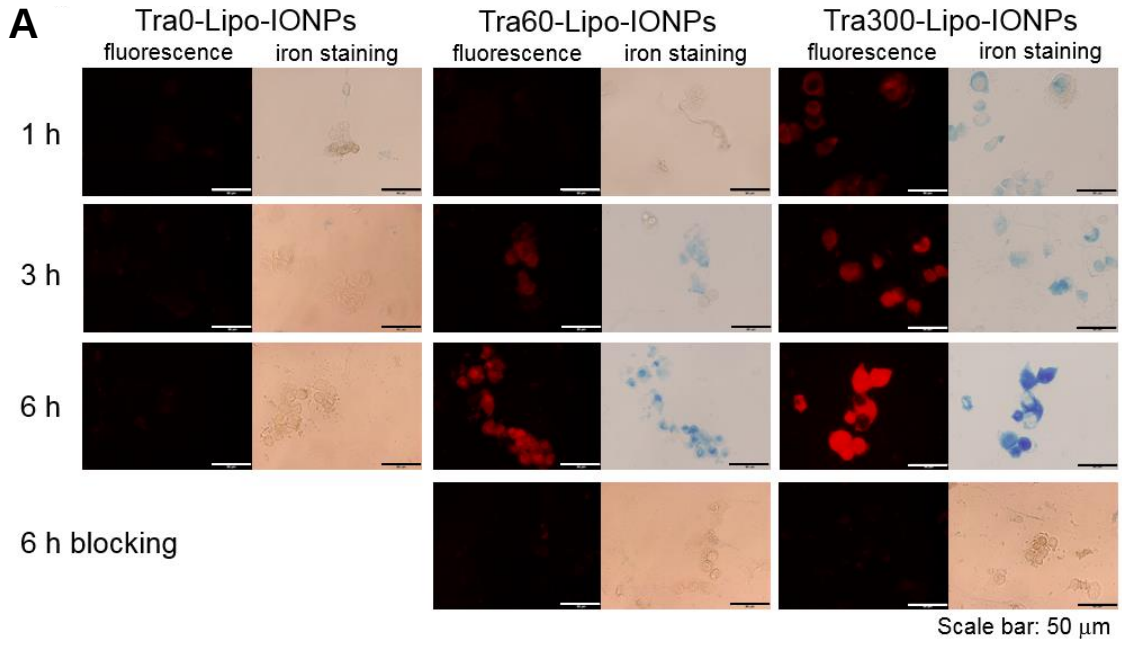

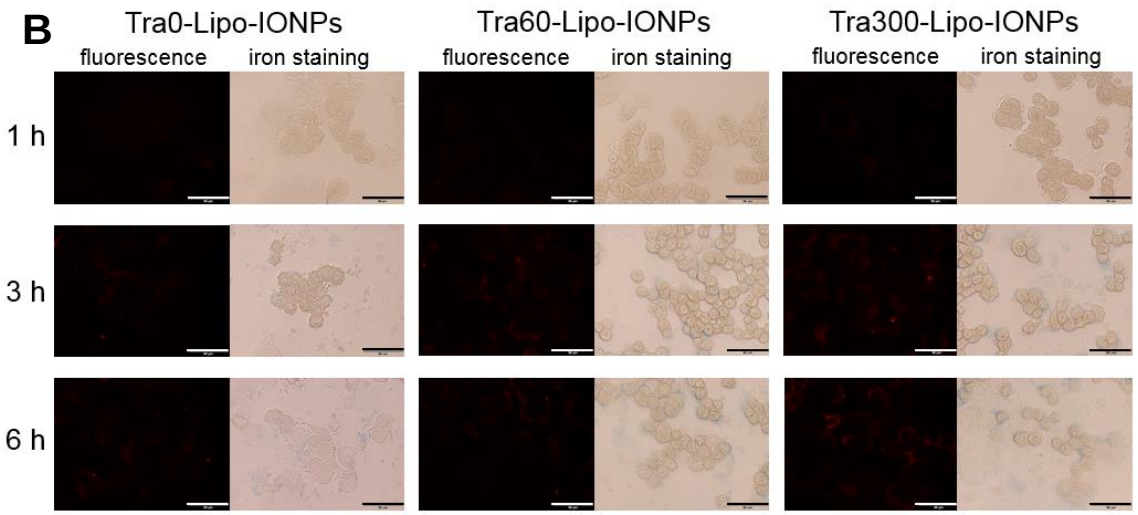

Figure 3-3. Fluorescence and iron staining images of N87 (A) and SUIT2 cells (B) incubated with Tra-Lipo-IONPs for 1, 3 and 6 h, and 6 h blocking. Scale bar = 50 μm.

3-1-5 *In vitro* cellular binding assay

The cellular binding of Tra-Lipo-IONPs was evaluated by measuring radioactivity of ^{125}I-labeled Tra-Lipo-IONPs taken up by the tumor cells, which is summarized in Figure 3-4. When ^{125}I-labeled Tra60-Lipo-IONPs and Tra300-Lipo-IONPs were added to N87 cells, the radioactivity bound to cells gradually increased over time. As the number of trastuzumab molecules conjugated to liposomes increased, higher binding of Tra-Lipo-IONPs to N87 cells was observed at each time point. On the other hand, there were no significant changes in radioactivity taken up by SUIT2 cells, even if the amount of trastuzumab bound to liposomes and incubation time were changed. The radioactivity of ^{125}I-labeled Tra60-Lipo-IONPs and Tra300-Lipo-IONPs in N87 cells when treated with overdosed trastuzumab was decreased to the same level as observed in SUIT2 cells at 6 h after incubation. These results agreed with those of our *in vitro* fluorescence microscopy study.

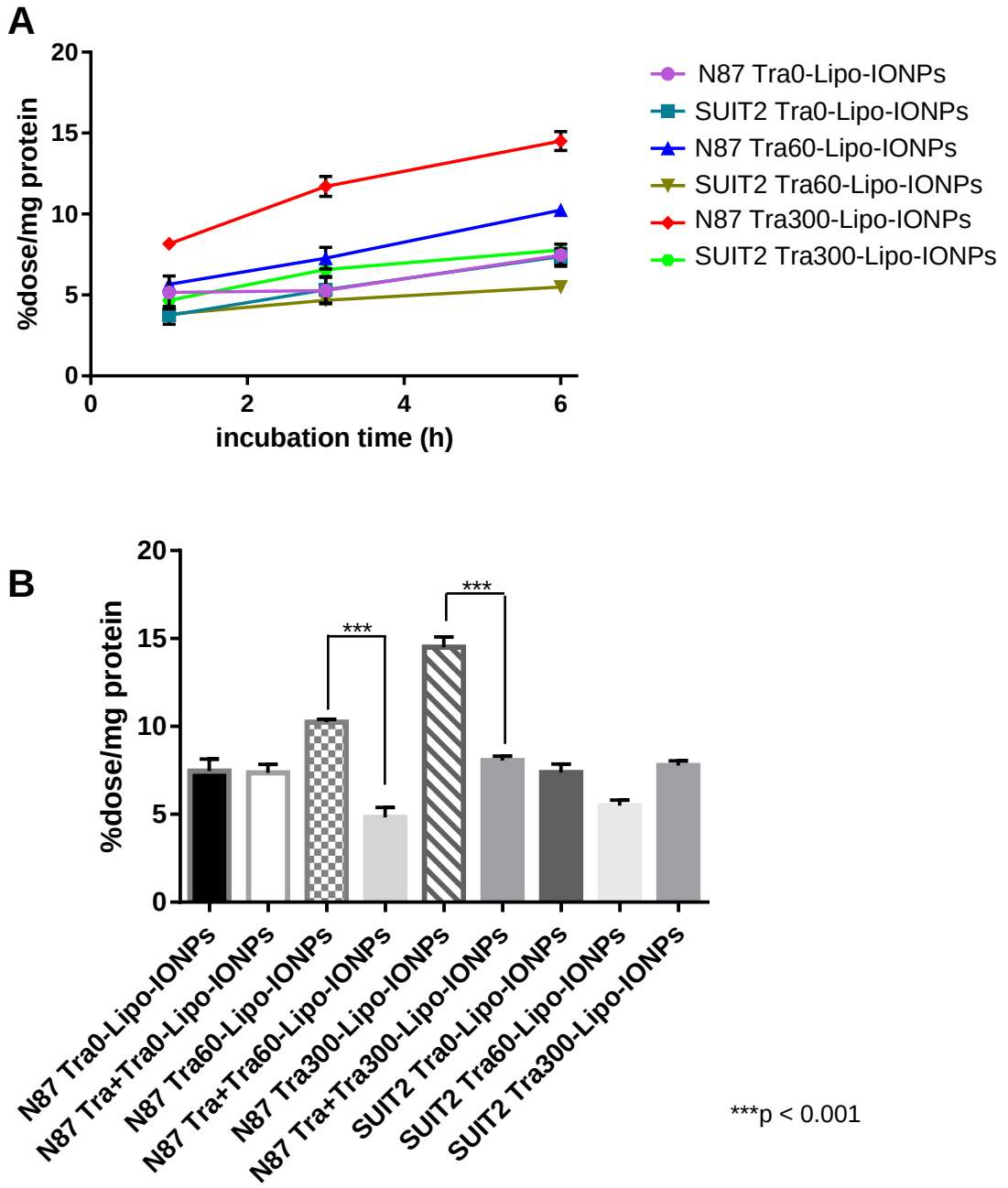

Figure 3-4. A. *In vitro* cellular binding of ^{125}I-labeled Tra0, 60, 300-Lipo-IONPs to N87 and SUIT2 cells at 1, 3, and 6 h after incubation (mean ± SD, n = 3).
B. *In vitro* cellular binding of ^{125}I-labeled Tra0, 60, 300-Lipo-IONPs to N87 cells and blocking at 6 h (mean ± SD, n = 3). ***p < 0.001.

3-1-6 *In vitro* PAI study

The cellular uptake of Tra300-Lipo-IONPs was evaluated by *in vitro* PAI using devices shown in

Figure 3-5. Distinctly increased PA signal was observed in N87 cells 6 h after incubation with Tra300-Lipo-IONPs, which was significantly decreased by co-treatment with overdosed trastuzumab, suggesting HER2-specific binding. Meanwhile, in the SUIT cells, only a minor increase in PA signal was detected at 6 h after incubation (Figure 3-6).

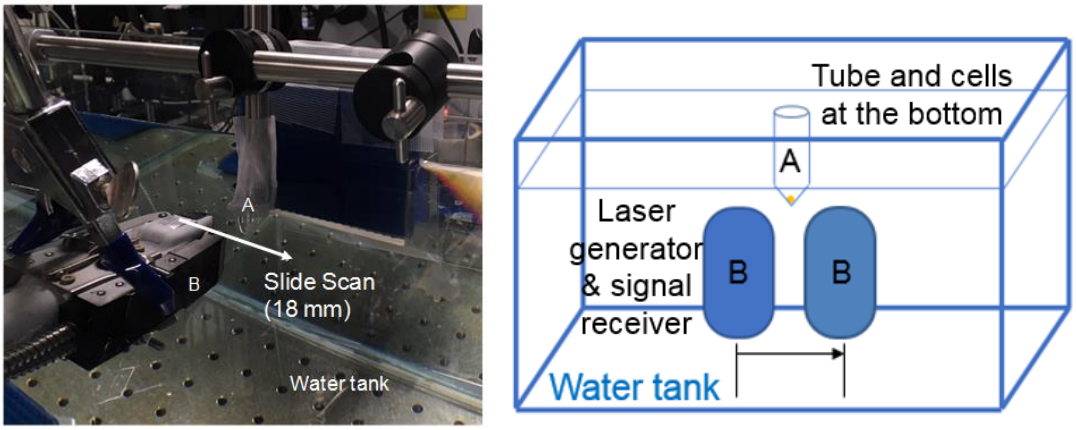

Figure 3-5. The photo and the graph demonstrate PA measuring instruments used for *in vitro* PAI.
A. Sample tube with cells at its bottom hangs over the water tank.
B. Laser generator and sensor, moving to take pictures of the sample.

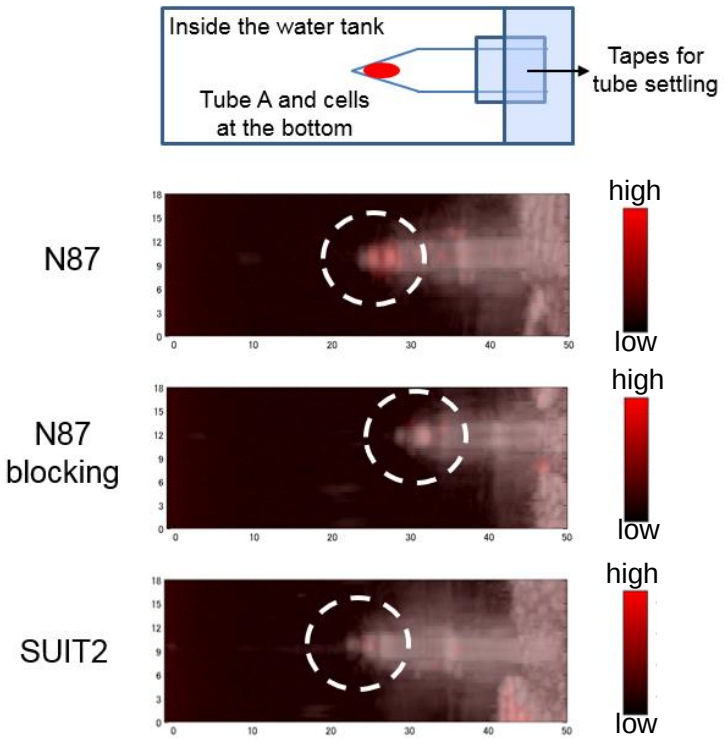

Figure 3-6. *In vitro* PAI study of Tra300-Lipo-IONPs. The white circle indicates collected N87 and SUIT2 cells in the tubes.

3-1-7 *In vitro* MRI study

The specific binding to HER2-overexpressing N87 cells by Tra-Lipo-IONPs was also demonstrated by *in vitro* MR studies. As described in Figure 3-7, N87 cells labeled with Tra60-Lipo-IONPs and Tra300-Lipo-IONPs displayed negative contrast enhancement in *T2*-weighted MRI images. The signal significantly decreased by 21.8 ± 0.6% and 51.6 ± 3.8% for Tra60-Lipo-IONPs and Tra300-Lipo-IONPs, respectively, compared to that in the control cells. This decrease in MRI signal was inhibited by co-incubation with overdosed trastuzumab. Meanwhile, there was no significant decrease in MRI signals for Tra0-Lipo-IONPs in N87 cells, as well as in all three kinds of Tra-Lipo-IONPs in SUIT2 cells. These results demonstrated that HER2-specific binding of Tra60, and 300-Lipo-IONPs *in vitro*, and that liposomes with more extensive trastuzumab conjugation bound more to cells expressing high levels of HER2.

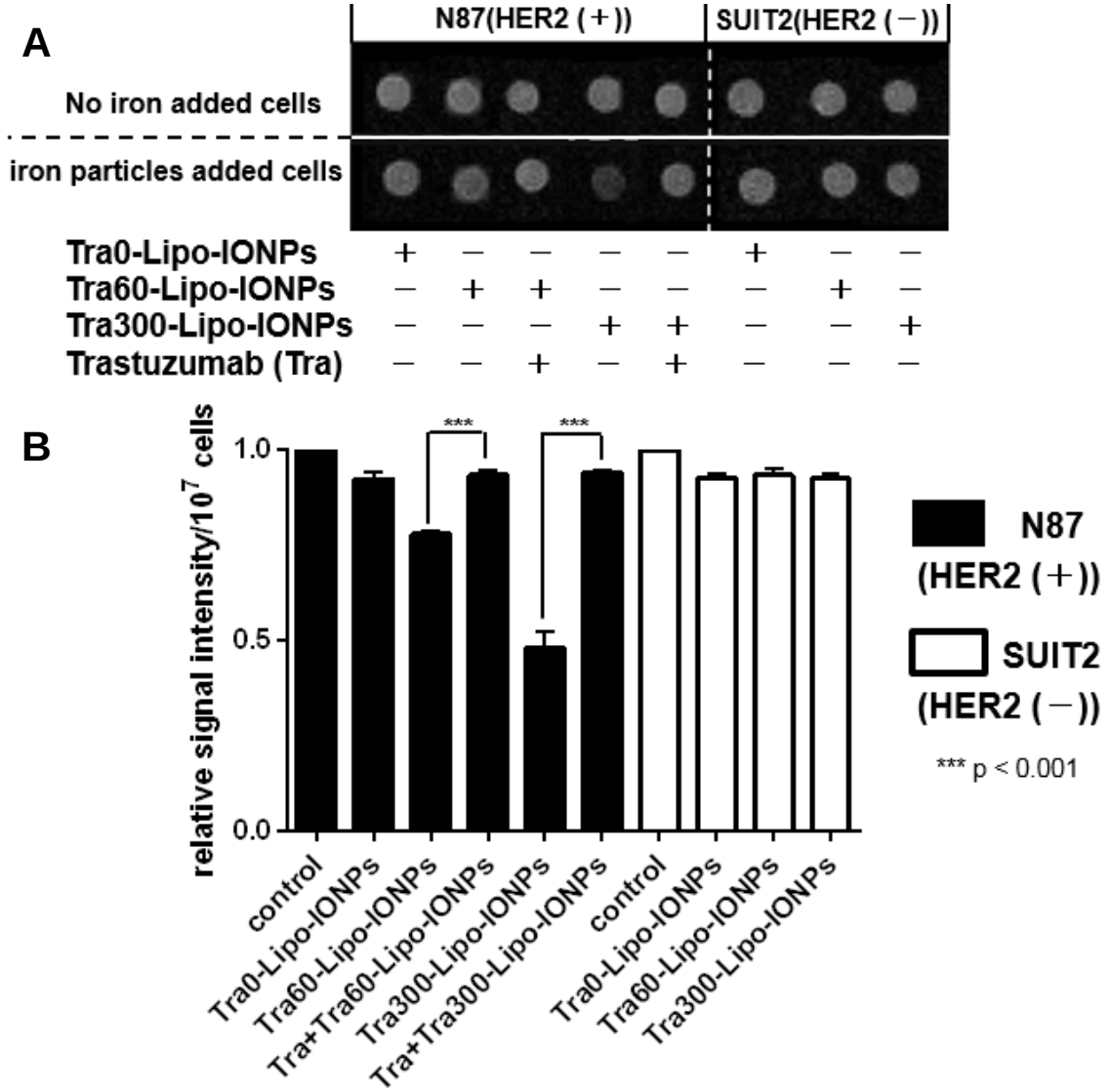

Figure 3-7. *In vitro* MRI study of Tra0, 60, 300-Lipo-IONPs.

A. Representative MR images of cells collected in tubes after 6 h incubation.

B. The relative MR signal intensity per 10^7 cells calculated from *in vitro* MR images (mean ± SD, n = 3). ***p < 0.001

3-1-8 Cellular uptake study (Tra-lipo-IONPs vs Tra-IONPs)

Although in phantom studies, Tra-lipo-IONPs showed a good signal enhancement, it is yet unknown if high sensitivity imaging can be achieved *in vitro* and *in vivo* as well. Thus, trastuzumab conjugated IONPs, or Tra-IONPs was prepared as a 'dispersed control' of Tra300-Lipo-IONPs.

The result showed the HER2 specific binding of Tra-IONPs (Figure 3-8). The uptake after 6 h

incubation was 19.2 %dose/mg protein, which was 1.3 times higher compared with Tra300-Lipo-IONPs. However, Tra300-Lipo-IONPs had 2.6- and 3.8-times PA and MR signals comparing to IONPs. Thus, if the %dose/mg protein was multiplied by the PA or MR signal, according to the results shown here, high sensitivity imaging would be achieved (Table 3-2).

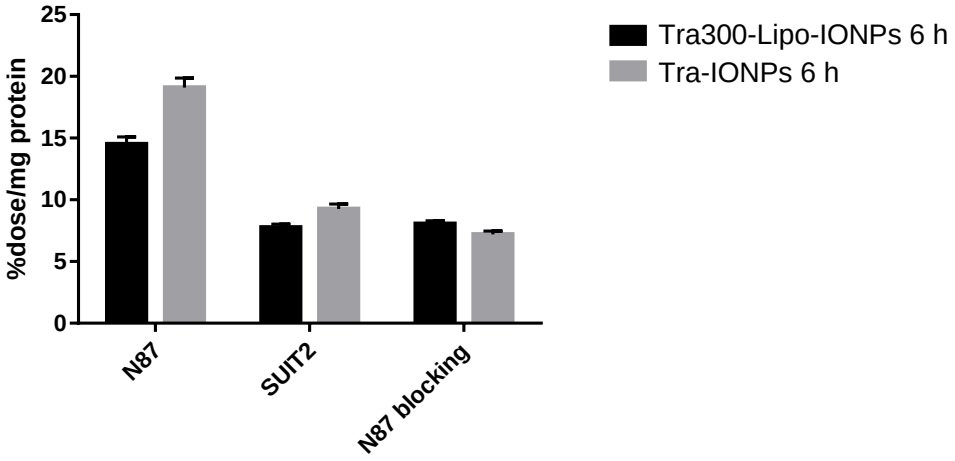

Figure 3-8. *In vitro* cellular binding of ^{125}I-labeled Tra-IONPs to N87 and SUIT2 cells at 6 h after incubation with or without trastuzumab blocking (mean ± SD, n = 3).

Table 3-2. Tra300-Lipo-IONPs vs Tra-IONPs on *in vitro* cellular binding and speculated PA and MR results.

	%dose/mg (6 h, N87)	PA signal (Tra-Lipo-IONPs vs IONPs)	MR signal (Tra-Lipo-IONPs vs IONPs)	%dose/mg × PA signal	%dose/mg × MR signal
Tra300-Lipo-IONPs	14.7	2.6	3.8	37.9	65.6
Tra-IONPs	19.2	1	1	19.2	19.2

3-1-9 Biodistribution study

Although the blood clearance was extremely rapid and a large amount of probes were taken up by the RES, at 1 h post-injection of Tra300-Lipo-IONPs, a significant difference between accumulation of N87 and SUIT2 tumors was observed (Figure 3-9A). Thus, HER2-specific binding of Tra300-Lipo-IONPs *in vivo* was indicated.

A comparison of the tumor accumulation at 1 h of dispersed Tra-IONPs showed that the

radioactivity accumulated in the N87 tumor was at nearly the same level, which was 1.5 and 1.9 %ID/g, respectively, whereas considering the PA signal generated by the probes, high sensitivity imaging was achieved by Tra300-Lipo-IONPs (Figure 3-9B, Table 3-3).

Furthermore, the tumor-to-blood ratio of Tra300-Lipo-IONPs in N87 was >1. According to a previous study[35], the tumor-to-blood ratio of Tra-IONPs after 1 h injection was only 0.26 (Figure 3-9C).

Although there is still room for improvement of tumor accumulation of Tra300-Lipo-IONPs, HER2-specific binding of Tra300-Lipo-IONPs *in vivo* was confirmed at 1 h post-injection. Furthermore, Tra-Lipo-IONPs showed higher tumor-to-blood ratios than those of Tra-IONPs, thus, Tra300-Lipo-IONPs were superior to Tra-IONPs as *in vivo* PA probes.

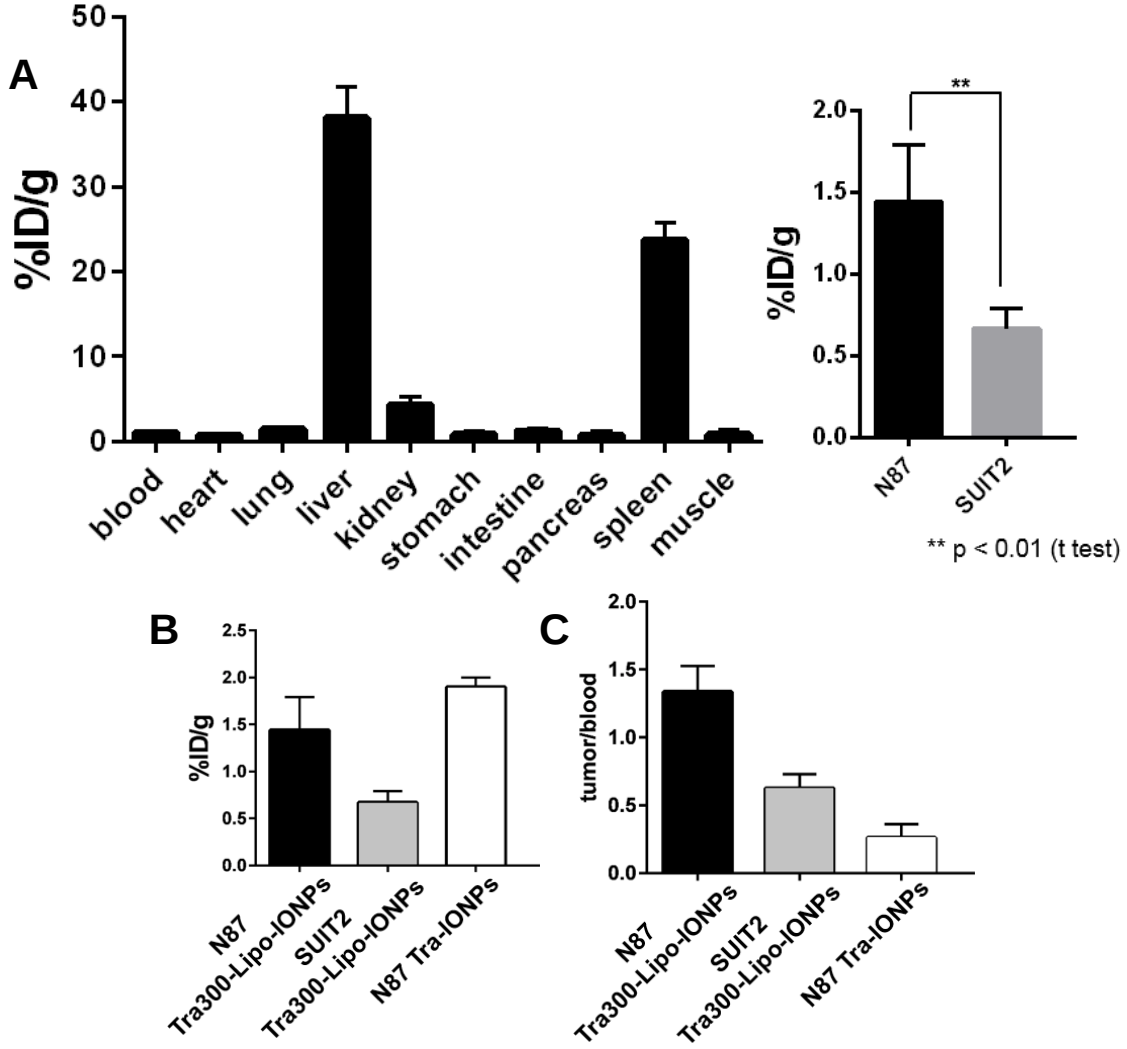

Figure 3-9. A. Biodistribution of radioactivity (%ID/g) 1 h after injection of ^{125}I-Tra300-Lipo-IONPs. (mean ± SD, n = 5)
B. The tumor uptake (mean ± SD) of ^{125}I-Tra300-Lipo-IONPs vs ^{111}In-Tra-IONPs (n = 3) 1 h after injection.
C. Tumor-to-blood ratios (mean ± SD) of ^{125}I-Tra300-Lipo-IONPs (n = 5) vs ^{111}In-Tra-IONPs (n = 3).

Table 3-3. Tra300-lipo-IONPs vs tra-IONPs on *in vivo* N87 tumor accumulation 1 h after injection and speculated PA results.

	%dose/mg (1 h, N87)	PA signal (Tra-Lipo-IONPs vs IONPs)	MR signal (Tra-Lipo-IONPs vs IONPs)	%dose/mg × PA signal	%dose/mg × MR signal
Tra300-Lipo-IONPs	1.5	2.6	3.8	3.87	5.7
Tra-IONPs	1.9	1	1	1.9	1.9

3-2 Summary

In this chapter, the author designed, synthesized, and evaluated a series of trastuzumab-conjugated liposomes with encapsulated IONPs at a high density in an interior aqueous phase (Tra-Lipo-IONPs) as sensitive PA/MR dual-imaging probes. The series had different amounts of trastuzumab conjugated to the liposome surface. The encapsulation was confirmed by TEM. Highly sensitive PA and MR signals were confirmed in PA and MR phantom studies, respectively. HER2-specific binding of Tra-Lipo-IONPs was proved in *in vitro* cellular uptake studies (measurement of radioactivity or fluorescence microscopy) as well as by PA and MR *in vitro* imaging. The probe with the most trastuzumab conjugation (Tra300-Lipo-IONPs) was chosen for further evaluation. In the *in vivo* biodistribution study, Tra300-Lipo-IONPs specifically accumulated in HER2-positive tumors at 1 h post-injection with a higher tumor-to-blood ratio than that of dispersed Tra-IONPs. These results suggest that Tra300-Lipo-IONPs has potential as a sensitive PA/MR dual imaging probe targeting HER2.

3-3 Experimental

3-3-1 Synthesis of Tra-Lipo-IONPs

Tra-Lipo-IONPs were prepared according to the following protocol, as previously described[46]. The IONPs (10 nm) (Ocean Nanotech, San Diego, USA) with carboxyl group modification was selected due to its negative surface charge. Fluorescent lipid (rhodamine-PE) was used to form the liposomes, with the aim of tracing them in subsequent experiments. Trastuzumab, at concentrations ranging from 0 to 300 μg/mL, was added to reactions in order to produce liposomes conjugated with different number of trastuzumab molecules. Tra-Lipo-IONPs were synthesized using [1,2-dipalmitoyl-sn-glycero-3-phosphocholine (DPPC) 28.6 mol%, cholesterol 32.6 mol%, ganglioside GM3 30.5 mol%, dicetyl phosphate (DCP) 4.1 mol%, 1,2-dipalmitoyl-sn-glycero-3-phosphorylehanolamine (DPPE) 4.2 mol%, rhodamine-PE 0.1 mol%], and 350 mg IONPs.

3-3-2 Physicochemical properties of Tra-Lipo-IONPs

The particle size and zeta potential of probes were measured with a Zetasizer Nano-ZSP instrument (Malvern Instruments, Ltd.). Total lipid concentrations of Tra-Lipo-IONPs were calculated on the basis of cholesterol concentration which was determined using a colorimetric enzymatic assay kit (cholesterol E-test kit) (Wako Pure Chemical Industries, Ltd.) in the presence of 0.125% sodium dodecyl sulfate.

Iron quantification was performed using IONPs (standard) serially diluted with HEPES buffer (0-5 mg Fe/mL). The standard samples and Tra-Lipo-IONPs were mixed with 1:1 methanol:chloroform solution to degrade liposomes, followed by absorbance measurements of both IONPs standard and Tra-Lipo-IONP samples at 376 nm.

The concentration of trastuzumab conjugated to liposomes was measured by Enzyme-Linked

ImmunoSorbent Assay (ELISA). The trastuzumab standard solution was serially diluted with PBS in a concentration range of 7.8-500 ng/mL. The standard samples and diluted Tra-Lipo-IONPs were immobilized on plates, followed by incubation at r.t. for 1 h. After blocking, anti-human IgG (Fc specific)-peroxidase was reacted. After washing, 1-Step Ultra TMB-ELISA (Thermo Fisher, Waltham, USA) was added, followed by measurement of absorbance at 450 nm after the reaction was stopped with addition of 2 M HCl.

3-3-3 TEM characterization

Tra0-Lipo-IONPs were embedded in a mixture of ethanol and Epon 812 epoxy embedding medium, and sliced samples were prepared. TEM images were taken using a Hitachi H7100 instrument (Hitachi, Tokyo, Japan).

3-3-4 Photoacoustic (PA) signal measurement

The IONPs and Tra0, 60, 300-Lipo-IONPs were diluted in PBS, with IONPs concentrations ranging from 0.00005 to 0.0008 mM (4.3 mM IONPs = 5 mg/mL iron). The measurement of PA signals was performed as previously described[37]. In brief, the PA signal measurement system consisted of pulsed light at 700-nm wavelength, generated by a Ti:Sapphire Laser system, Model LT-2211-PC (Lotis TII, Minsk, Belarus) and operating at 10 Hz with 20 ns pulse duration. A transducer, Model V303 (Panametrics-NDT, Waltham, MA, USA) with 1-MHz center frequency and 1 cm element size, and an ultrasonic preamplifier, Model 5682 (Olympus Corporation, Tokyo, Japan), collected the PA signal. DPO4104 (Tektronix Company, Beaverton, OR, USA) was used as a gauge; light detection by a Si-biased detector, DET10A/M (Thorlabs, Newton, NJ, USA) was a trigger. PA signal intensity was normalized by both the pulsed-light intensity and the sample concentration.

3-3-5 Calculation of *r2*

The IONPs and Tra0, 60, 300-Lipo-IONPs were diluted in PBS, with iron concentrations ranging from 0 to 0.2 mM. The transverse relaxivity (*r2*) was measured using an MRI system (MRmini SA (1.5 T)) in the same condition described in the Chapter 2. The *r2* was obtained from the slope of the regression line between *R2* and concentrations of IONPs or Tra-Lipo-IONPs.

3-3-6 Cell culture

Cell culture of N87 and SUIT2 cells were performed according to the method in Chapter 1.

3-3-7 *In vitro* fluorescence microscopy study

N87 and SUIT2 cells (5×10^4) were seeded in a multi-well glass-bottom dish (Matsunami Glass, Osaka, Japan) and incubated for 24 h at 37°C and 5% CO_2. The cells were washed with PBS before Tra-Lipo-IONPs (0.1 mL FBS-free DMEM) were added. The iron concentration of Tra-Lipo-IONPs solution added to cells was 0.2 mg/mL. For blocking studies, a mixture of overdosed trastuzumab (0.24 mg for Tra60-Lipo-IONPs and 1.2 mg for Tra300-Lipo-IONPs) and Tra-Lipo-IONPs was added to cells. Cells were incubated for 1, 3, and 6 h at 37°C under 5% CO_2, followed by washing three times with PBS. Fluorescence microscopy was performed using an Olympus X81 microscope (Olympus America, Inc., NY, USA) at an exposure time of 1/6 s, followed by cell iron staining using Berlin blue staining set (Wako Pure Chemical Industries, Ltd.).

3-3-8 ^{125}I-labeling of Tra-Lipo-IONPs

N-Succinimidyl 3-[^{125}I]iodobenzoate ([^{125}I]SIB) was synthesized according to a previous report[47]. The [^{125}I]SIB solution was evaporated by N_2 gas, then mixed with Tra-Lipo-IONP dissolved in phosphate buffer (0.1 M, pH 8.6). After incubation at r.t. for 40 min, the mixture was purified using

size-exclusion column chromatography (PD-10 columns, GE Healthcare UK Ltd., Buckinghamshire, UK), and concentrated by centrifugal filtration (Amicon Ultra-4, 30 kDa). Radiochemical purity was analyzed by PD-10 column (GE Healthcare).

3-3-9 *In vitro* cellular binding assay

N87 and SUIT2 cells (2×10^5) were seeded in 24-well plates and incubated for 16 h at 37°C under 5% CO_2. ^{125}I-labeled Tra-Lipo-IONPs solution was added to cells at an iron concentration of 0.03 mg/mL. For blocking studies (6 h), overdosed trastuzumab (0.11 mg for Tra60-Lipo-IONPs and 0.55 mg for Tra300-Lipo-IONPs) was mixed with Tra-Lipo-IONPs before being added to cells. Cells were incubated for 1, 3, and 6 h at 37°C under 5% CO_2, followed by washing four times with PBS. The cells were then lysed with 1 N NaOH and incubated at 37°C for 1 h. The radioactivity bound to the cells was measured with a γ-counter (1470 WIZARD), followed by the measurement of protein concentration using a BCA protein assay kit (Thermo Fisher Scientific Inc.). The uptake of ^{125}I-labeled Tra-Lipo-IONPs was represented as the percentage dose/mg protein.

3-3-10 *In vitro* PAI

N87 and SUIT2 cells (1×10^6) were seeded in 6-well plates and incubated for 16 h at 37°C under 5% CO_2. Tra300-Lipo-IONPs solution was added to cells at an iron concentration of 0.2 mg/mL. Overdosed trastuzumab was mixed with Tra300-Lipo-IONPs before addition to cells for blocking studies. Cells were incubated for 6 h at 37°C under 5% CO_2, followed by washing three times with PBS. The cells were then collected in 0.5 mL tubes to be imaged. The PA instruments were set as demonstrated in Figure 3-5. The tube was suspended in water, and custom optical fibers (NA = 0.22, core diameter 230 μm, Mitsubishi Cable Industries, Tokyo, Japan) and an ultrasound linear array probe, SL15-4 (center frequency 8 MHz, SuperSonic Imagine, Aix-en-Provence, France) was used to

take ultrasound images. We used an ultrasound system, Aixplorer (SuperSonic Imagine), as an ultrasound device.

3-3-11 *In vitro* MR imaging

After N87 or SUIT-2 cells were cultured in 75 cm^2 flasks (1.3×10^7 cells) for 16 h. Tra-Lipo-IONPs in FBS-free DMEM medium were added to the flask (m_{iron} = 2 μg). For blocking studies, overdosed trastuzumab (24 μg for Tra60-Lipo-IONPs and 120 μg for Tra300-Lipo-IONPs) was mixed with Tra-Lipo-IONPs in FBS-free DMEM medium. After incubation at 37°C for 6 h, 1×10^7 cells were collected in 0.5 mL tubes for imaging. N87 or SUIT2 cells without IONPs incubation were collected as controls. Centrifuged cells were placed into the φ38.5 mm RF coil of MRmini SA, and images were taken and analyzed, as described in the Chapter 2.

3-3-12 Tra-IONPs cell binding study

IONPs with carboxyl groups (Iron oxide magnetic nanoparticles solution, Sigma-Aldrich, St. Louis, Missouri, USA) on surface was activated by EDC/NHS as described in Chapter 1 and reacted with ^{125}I-labeled trastuzumab.

N87 and SUIT2 cells were seeded in 24-well plates (2×10^5 cells/well) and incubated for 16 h. ^{125}I-Tra-IONPs (0.03 mg/mL) was added to cells followed by 6 h incubation. Blocking was performed with excess (10000-fold) trastuzumab. Cells were lysed using NaOH, radioactivity and protein concentration were measured as in *in vitro* cellular binding assay.

3-3-13 Animal models

N87 and SUIT2 tumors-bearing mice were prepared according to the method in Chapters 1 and 2.

3-3-14 Biodistribution study

^{125}I-labeled Tra300-Lipo-IONP (iron amount 100 μg/mouse, 2.5-4.9 μCi/mouse) was dissolved into PBS and administrated to N87 and SUIT2 tumor bearing mice intravenously. The biodistribution was monitored at 1 h post-injection (n = 5). Organs of interest were excised, weighed, and radioactivity counts were determined with a γ-counter using the injected dose as a standard. Data were calculated as the percentage injected dose per gram of tissue (%ID/g) except for thyroid (%ID).

3-3-15 Statistical Analysis

Each experiment was individually performed at least three times. The statistical significance among groups was identified using Dunnett's test and t test. Data are presented as the mean ± standard deviation. P values of less than 0.05 were considered statistically significant.

Conclusion

In the present study, the author reaches a conclusion as follows.

1) In Chapter 1, based on gold nanorods (AuNRs), a series of trastuzumab-conjugated AuNRs with different amounts of ligand conjugation was synthesized and evaluated as potential PA/SPECT dual-imaging probes. Among the series, Tra2-AuNRs showed the best selective accumulation to HER2-positive N87 tumors in biodistribution studies as well as good affinity to N87 cells. Tra2-AuNRs also achieved N87-selective tumor imaging 96 h after probe injection in a SPECT study. These results suggested that Tra2-AuNRs may be a PA/SPECT dual imaging probe targeting HER2-positive tumors.
2) In Chapter 2, to achieve high-contrast *in vivo* imaging of HER2 at an earlier time point post-injection, iron oxide nanoparticles (IONPs) were used instead of AuNRs as the probe vehicle. Because IONPs are used as *T2*-weighted contrast agent in MRI, they were evaluated as a potential PA/MR dual-imaging probe. Anti-HER2 single chain Fv (scFv)-conjugated IONPs showed high binding affinity toward HER2 as well as HER2 selective PA/MR dual imaging both *in vitro* and *in vivo,* which indicated its potential usage as a robust cancer-targeted PA/MR dual imaging probe.
3) In Chapter 3, to achieve highly sensitive PA signals, we used trastuzumab-conjugated liposomes encapsulating IONPs at a high density (Tra-Lipo-IONPs). A series of liposomes with different amounts of ligand conjugation were designed, synthesized and evaluated. Significantly higher PA and MR signals for these liposomes than for dispersed IONPs were observed. Among the series, Tra300-Lipo-IONPs showed the highest binding affinity and HER2-specific PA/MR imaging *in vitro*. Tra300-Lipo-IONPs also specifically accumulated in HER2-positive tumors at 1 h post-injection with higher tumor-to-blood ratios than those achieved with dispersed Tra-IONPs. These results suggest that Tra300-Lipo-IONPs have a potential as a sensitive PA/MR dual imaging probe

targeting HER2.

In this thesis, the author developed pre-operative and intra-operative dual-imaging probes based on metal nanoparticles (AuNRs and IONPs) targeting HER2. Among all the probes discussed, Tra300-Lipo-IONPs showed the best potential as a pre-operative (MR) and intra-operative (PA) probe for HER2-targeted tumor imaging. These data provide useful information for the development of imaging probes applicable for pre- and intra-operative diagnoses and precise cancer therapy.

References

1. Bray, F., Ferlay, J., Soerjomataram, I., Siegel, R. L., Torre, L. A., Jemal, A. (2018). Global cancer statistics 2018: GLOBOCAN estimates of incidence and mortality worldwide for 36 cancers in 185 countries. CA: a Cancer Journal for Clinicians, 68(6), 394-424.
2. Nagao, M., Tsugane, S. (2016). Cancer in Japan: prevalence, prevention and the role of heterocyclic amines in human carcinogenesis. Genes and Environment, 38(1), 16-23.
3. Aliperti, L. A., Predina, J. D., Vachani, A., Singhal, S. (2011). Local and systemic recurrence is the Achilles heel of cancer surgery. Annals of Surgical Oncology, 18(3), 603-607.
4. Jiang, J. X., Keating, J. J., De Jesus, E. M., Judy, R. P., Madajewski, B., Venegas, O., Okusanya, O.T., Singhal, S. (2015). Optimization of the enhanced permeability and retention effect for near-infrared imaging of solid tumors with indocyanine green. American Journal of Nuclear Medicine and Molecular Imaging, 5(4), 390-400.
5. Tanaka, T., Terai, Y., Ono, Y. J., Fujiwara, S., Tanaka, Y., Sasaki, H., Tsunetoh, S., Kanemura, M., Yamamoto, K., Yamamoto, T., Ohmichi, M. (2015). Preoperative MRI and intraoperative frozen section diagnosis of myometrial invasion in patients with endometrial cancer. International Journal of Gynecological Cancer, 25(5), 879-883.
6. Arita, J., Ono, Y., Takahashi, M., Inoue, Y., Takahashi, Y., Matsueda, K., Saiura, A. (2015). Routine preoperative liver-specific magnetic resonance imaging does not exclude the necessity of contrast-enhanced intraoperative ultrasound in hepatic resection for colorectal liver metastasis. Annals of Surgery, 262(6), 1086-1091.
7. Xiao, Q., Chen, T., Chen, S. (2018). Fluorescent contrast agents for tumor surgery. Experimental and Therapeutic Medicine, 16(3), 1577-1585.
8. Nie, J., Zhang, J., Gao, J., Guo, L., Zhou, H., Hu, Y., Zhu, C., Li, Q., Ma, X. (2017). Diagnostic role of ^{18}F-FDG PET/MRI in patients with gynecological malignancies of the pelvis: A systematic review and meta-analysis. PloS One, 12(5), e0175401.
9. Zhu, D., Wang, L., Zhang, H., Chen, J., Wang, Y., Byanju, S., Liao, M. (2017). Prognostic value of ^{18}F-FDG-PET/CT parameters in patients with pancreatic carcinoma: A systematic review and meta-analysis. Medicine, 96(33), e7813.
10. Nomori, H., Cong, Y., Sugimura, H. (2016). Utility and pitfalls of sentinel node identification using indocyanine green during segmentectomy for cT1N0M0 non-small cell lung cancer. Surgery Today, 46(8), 908-913.
11. Kim, H. K., Quan, Y. H., Choi, B. H., Park, J. H., Han, K. N., Choi, Y., Kim, B. M., Choi, Y. H. (2015). Intraoperative pulmonary neoplasm identification using near-infrared fluorescence imaging. European Journal of Cardio-Thoracic Surgery, 49(5), 1497-1502.

12. Tam, A. C. (1986). Applications of photoacoustic sensing techniques. Reviews of Modern Physics, 58(2), 381-431.
13. Kanazaki, K., Sano, K., Makino, A., Yamauchi, F., Takahashi, A., Homma, T., Ono, M., Saji, H. (2016). Feasibility of poly (ethylene glycol) derivatives as diagnostic drug carriers for tumor imaging. Journal of Controlled Release, 226, 115-123.
14. Jain, P. K., Lee, K. S., El-Sayed, I. H., El-Sayed, M. A. (2006). Calculated absorption and scattering properties of gold nanoparticles of different size, shape, and composition: applications in biological imaging and biomedicine. The Journal of Physical Chemistry B, 110(14), 7238-7248.
15. Matsumura, Y., Maeda, H. (1986). A new concept for macromolecular therapeutics in cancer chemotherapy: mechanism of tumoritropic accumulation of proteins and the antitumor agent smancs. Cancer Research, 46(12 Part 1), 6387-6392.
16. Pouliquen, D., Le Jeune, J. J., Perdrisot, R., Ermias, A., Jallet, P. (1991). Iron oxide nanoparticles for use as an MRI contrast agent: pharmacokinetics and metabolism. Magnetic Resonance Imaging, 9(3), 275-283.
17. Slamon, D. J., Godolphin, W., Jones, L. A., Holt, J. A., Wong, S. G., Keith, D. E., Levin, W. J., Stuart, S. G., Udove, J., Ullrich, A. (1989). Studies of the HER-2/neu proto-oncogene in human breast and ovarian cancer. Science, 244(4905), 707-712.
18. Hori, M., Matsuda, T., Shibata, A., Katanoda, K., Sobue, T., Nishimoto, H., Japan Cancer Surveillance Research Group (2015). Cancer incidence and incidence rates in Japan in 2009: a study of 32 population-based cancer registries for the Monitoring of Cancer Incidence in Japan (MCIJ) project. Japanese Journal of Clinical Oncology, 45(9):884-891.
19. Luo, G. F., Chen, W. H., Lei, Q., Qiu, W. X., Liu, Y. X., Cheng, Y. J., Zhang, X. Z. (2016). A triple-collaborative strategy for high-performance tumor therapy by multifunctional mesoporous silica-coated gold nanorods. Advanced Functional Materials, 26(24), 4339-4350.
20. Zhang, P., Wang, Y., Lian, J., Shen, Q., Wang, C., Ma, B., Zhang, Y., Xu, T., Li, J., Shao, Y., Xu, F., Zhu, J. J. (2017). Engineering the surface of smart nanocarriers using a pH-/thermal-/GSH-responsive polymer zipper for precise tumor targeting therapy *in vivo*. Advanced Materials, 29(36), 1702311-1702320.
21. Zhao, X., Yang, C. X., Chen, L. G., Yan, X. P. (2017). Dual-stimuli responsive and reversibly activatable theranostic nanoprobe for precision tumor-targeting and fluorescence-guided photothermal therapy. Nature Communications, 8, 14998-15006.
22. Mamot, C., Ritschard, R., Wicki, A., Stehle, G., Dieterle, T., Bubendorf, L., Hilker, C., Hilker, S., Herrmann, R.,Rochlitz, C. (2012). Tolerability, safety, pharmacokinetics, and efficacy of doxorubicin-loaded anti-EGFR immunoliposomes in advanced solid tumours: a phase 1 dose-escalation study. The Lancet Oncology, 13(12), 1234-1241.
23. Kennedy, L. C., Bickford, L. R., Lewinski, N. A., Coughlin, A. J., Hu, Y., Day, E. S., West, J. L.,

Drezek, R. A. (2011). A new era for cancer treatment: gold‐nanoparticle‐mediated thermal therapies. Small, 7(2), 169-183.

24. Sano, K., Ohashi, M., Kanazaki, K., Ding, N., Deguchi, J., Kanada, Y., Ono, M., Saji, H. (2015). *In vivo* photoacoustic imaging of cancer using indocyanine green-labeled monoclonal antibody targeting the epidermal growth factor receptor. Biochemical and biophysical research communications, 464(3), 820-825.
25. Chauhan, V. P., Jain, R. K. (2013). Strategies for advancing cancer nanomedicine. Nature Materials, 12(11), 958-962.
26. An, L., Wang, Y., Tian, Q., Yang, S. (2017). Small gold nanorods: Recent advances in synthesis, biological imaging, and cancer therapy. Materials, 10(12), 1372.
27. Martínez, J. C., Chequer, N. A., González, J. L., Cordova, T. (2012). Alternative metodology for gold nanoparticles diameter characterization using PCA technique and UV-Vis spectrophotometry. Nanoscience and Nanotechnology, 2(6), 184-189.
28. Wagner, V., Dullaart, A., Bock, A. K., Zweck, A. (2006). The emerging nanomedicine landscape. Nature Biotechnology, 24(10), 1211-1217.
29. Wang, Y. X. J., Hussain, S. M., Krestin, G. P. (2001). Superparamagnetic iron oxide contrast agents: physicochemical characteristics and applications in MR imaging. European Radiology, 11(11), 2319-2331.
30. J Wang, Y. X., Xuan, S., Port, M., Idee, J. M. (2013). Recent advances in superparamagnetic iron oxide nanoparticles for cellular imaging and targeted therapy research. Current Pharmaceutical Design, 19(37), 6575-6593.
31. Ittrich, H., Peldschus, K., Raabe, N., Kaul, M., Adam, G. (2013). Superparamagnetic iron oxide nanoparticles in biomedicine: applications and developments in diagnostics and therapy. RöFo-Fortschritte auf dem Gebiet der Röntgenstrahlen und der bildgebenden Verfahren, 185(12), 1149-1166.
32. Wahajuddin, S. A. (2012). Superparamagnetic iron oxide nanoparticles: magnetic nanoplatforms as drug carriers. International Journal of Nanomedicine, 7, 3445-3471.
33. Rudin, M., Rausch, M., Stoeckli, M. (2005). Molecular imaging in drug discovery and development: potential and limitations of nonnuclear methods. Molecular Imaging and Biology, 7(1), 5-13.
34. Armanetti, P., Flori, A., Avigo, C., Conti, L., Valtancoli, B., Petroni, D., Doumettd, S., Cappiellod, L., Cappiellod, C., Baldid, G., Bencinic, A., Menichetti, L. (2018). Spectroscopic and photoacoustic characterization of encapsulated iron oxide super-paramagnetic nanoparticles as a new multiplatform contrast agent. Spectrochimica Acta Part A: Molecular and Biomolecular Spectroscopy, 199, 248-253.
35. Moore, A., Weissleder, R., Bogdanov Jr, A. (1997). Uptake of dextran- coated monocrystalline

iron oxides in tumor cells and macrophages. Journal of Magnetic Resonance Imaging, 7(6), 1140-1145.

36. Keliher, E. J., Yoo, J., Nahrendorf, M., Lewis, J. S., Marinelli, B., Newton, A., Pittet, M. J., Weissleder, R. (2011). ^{89}Zr-labeled dextran nanoparticles allow *in vivo* macrophage imaging. Bioconjugate Chemistry, 22(12), 2383-2389.
37. Kanazaki, K., Sano, K., Makino, A., Shimizu, Y., Yamauchi, F., Ogawa, S., Ding, N., Yano, T., Temma, T., Ono, M.,Saji, H. (2015). Development of anti-HER2 fragment antibody conjugated to iron oxide nanoparticles for *in vivo* HER2-targeted photoacoustic tumor imaging. Nanomedicine: Nanotechnology, Biology and Medicine, 11(8), 2051-2060.
38. Ding, N., Sano, K., Kanazaki, K., Ohashi, M., Deguchi, J., Kanada, Y., Ono, M., Saji, H. (2016). *In vivo* HER2-targeted magnetic resonance tumor imaging using iron oxide nanoparticles conjugated with anti-HER2 fragment antibody. Molecular Imaging and Biology, 18(6), 870-876.
39. Ju, K. Y., Kang, J., Pyo, J., Lim, J., Chang, J. H., Lee, J. K. (2016). pH-Induced aggregated melanin nanoparticles for photoacoustic signal amplification. Nanoscale, 8(30), 14448-14456.
40. Bayer, C. L., Nam, S. Y., Chen, Y. S., Emelianov, S. Y. (2013). Photoacoustic signal amplification through plasmonic nanoparticle aggregation. Journal of Biomedical Optics, 18(1), 016001.
41. Smith, B. R., Gambhir, S. S. (2017). Nanomaterials for *in vivo* imaging. Chemical Reviews, 117(3), 901-986.
42. Willets, K. A., Stranahan, S. M., Weber, M. L. (2012). Shedding light on surface-enhanced Raman scattering hot spots through single-molecule super-resolution imaging. The Journal of Physical Chemistry Letters, 3(10), 1286-1294.
43. Cheng, K., Kothapalli, S. R., Liu, H., Koh, A. L., Jokerst, J. V., Jiang, H., Yang, M., Li, J., Levi, J., Wu, J. C., Gambhir, S. S., Cheng, Z. (2014). Construction and validation of nano gold tripods for molecular imaging of living subjects. Journal of the American Chemical Society, 136(9), 3560-3571.
44. Tromsdorf, U. I., Bigall, N. C., Kaul, M. G., Bruns, O. T., Nikolic, M. S., Mollwitz, B., Sperling, R. A., Reimer, R., Hohenberg, H., Parak, W. J., Förster, S., Beisiegel, U., Adam, G., Weller, H.(2007). Size and surface effects on the MRI relaxivity of manganese ferrite nanoparticle contrast agents. Nano Letters, 7(8), 2422-2427.
45. Jun, Y. W., Huh, Y. M., Choi, J. S., Lee, J. H., Song, H. T., Yoon, S., Kim, K. S., Shin, J. S., Suh, J. S., Cheon, J. (2005). Nanoscale size effect of magnetic nanocrystals and their utilization for cancer diagnosis via magnetic resonance imaging. Journal of the American Chemical Society, 127(16), 5732-5733.
46. Minematsu, H., Otani, T., Oohashi, T., Hirai, M., Oie, K., Igarashi, K., & Ohtsuka, A. (2010). Development of an active targeting liposome encapsulated with high-density colloidal gold for transmission electron microscopy. Journal of electron microscopy, 60(1), 95-99.

47. Sano, K., Temma, T., Kuge, Y., Kudo, T., Kamihashi, J., Zhao, S., Saji, H. (2010). Radioimmunodetection of membrane type-1 matrix metalloproteinase relevant to tumor malignancy with a pre-targeting method. Biological and Pharmaceutical Bulletin, 33(9), 1589-1595.

Acknowledgements

I am extremely lucky to have had the chance to work with Professor Hideo Saji, Professor Masahiro Ono and Dr. Kohei Sano on the ideas in this dissertation, and I would very much like to thank them for their support. Professor Saji took me on as a graduate student, opened the door towards the patho-functional bioanalysis field, and encouraged me to pursue the goal that I had a passion for. Dr. Sano is the one that originally drew me to the development of cancer imaging. Dr. Sano instructed me from the very base of research and inspired me hugely with his contagious enthusiasm and outlook on research. I could not have asked for a better mentor and I feel very grateful from the bottom of my heart for his generosity with his time, experience and thoughts. I would also like to thank Professor Ono, who gave me constructive ideas and suggestions constantly through the years both academically and in life, and who was always generous with his time.

I am grateful to Dr. Yoichi Shimizu and Dr. Hiroyuki Watanabe for consistently sharing practical and thoughtful advices. Thanks also to Dr. Hiroyuki Kimura for all the help he offered concerning the operation of MRI related devices.

I would also like to thank Dr. Kengo Kanazaki for having taught me many experimental techniques and have given me many experimental suggestions, as well as Professor Takeshi Namita, Graduate School of Medicine, for all the help and support provided on PA experiments.

I would like to thank all my wonderful friends and colleagues at the Patho-functional bioanalysis lab. I would especially like to thank Manami Ohashi, Yuko Kanada and Jun Deguchi for all those helpful discussions and suggestions, and for having helped make my days in the lab enjoyable. I would also like to thank Ms. Aya Ono for helping me start daily life in Japan smoothly, and Ms. Saeko Terai for all the help on RI related routines. Thanks also to other colleagues in the lab, including Dr. Shinpei Iikuni, Haruka Okuda, Yuki Doi, Sho Kaide, Masaru Fujinohara, Naoki Mastushita, Yuya Okada,

Kiyoshiro Kawano, Kouji Mastuyoshi, Yusuke Miki, Keiichi Tanimura, Kengo Fukui, Futa Itagaki, Shiori Sakai, Haruka Tastumi, Yukihiro Nakai, Masato Ando, Yuki Idoko, Ichiro Kamei, Mari Suzukita, Yuuta Tarumizu.

Thank you to Victor Hugo, Alan Rickman, J.K.Rowling and Lin-Manuel Miranda for your absolute talent and humanity, and for inspiring me to create a vision for life. To Mat Baynton and Jonny Phillips for the laughter and happy memories. To my dearest friends Chunjiao Zhou, Ting Xiao, Hongxue Ni and Xueming Xia for your time, love, thoughts and company. You kept me alive.

Finally, I would like to thank my parents for their love and support. I simply cannot think of anyone more supportive for providing me with guidance and encouragement and allowing me to be what I was always meant to be.